André Miguel
Labrincha Barreirinha

Monitorização da produtividade da vegetação em áreas de maior suscetibilidade de ocorrência de fogos severos em Portugal Continental.

Monitoring of vegetation productivity in areas of higher susceptibility to severe fires in mainland Portugal.

Universidade de Aveiro
2022

André Miguel Labrincha Barreirinha

Monitorização da produtividade da vegetação em áreas de maior suscetibilidade de ocorrência de fogos severos em Portugal Continental.

Monitoring of vegetation productivity in areas of higher susceptibility to severe fires in mainland Portugal.

Dissertação apresentada à Universidade de Aveiro para cumprimento dos requisitos necessários à obtenção do grau de Mestre em Ciências do Mar e da Atmosfera, realizada sob a orientação científica do Doutor José Manuel Henriques Castanheira, Professor Auxiliar do Departamento de Física da Universidade de Aveiro, e da Doutora Célia Marina Pedroso Gouveia, Professora Auxiliar Convidada do Departamento de Engenharia Geográfica, Geofísica e Energia da Universidade de Lisboa.

o júri / the jury

presidente / president

Prof. Doutor Carlos Manuel Martins Santos Fonseca
Professor Associado Convidado C/ Agregação, Universidade de Aveiro

vogais / examiners committee

Prof. Doutor Carlos do Carmo de Portugal e Castro da Camara
Professor Associado, Faculdade de Ciências da Universidade de Lisboa

Doutora Célia Marina Pedroso Gouveia
Professora Auxiliar Convidada, Faculdade de Ciências da Universidade de Lisboa

agradecimentos / acknowledgements

I'm extremely grateful to my supervisors, Prof. José Castanheira and Prof. Célia Gouveia for their help, guidance and availability during this year of work. I would also like to emphasize the role of Prof. José Castanheira not only this last year but also during my academic career as he also supervised me during the Bachelor Project and helped me multiple times in other works.

I am also thankful to Tiago Silva for his help with the Burned Area data and with the download of some of the other datasets used.

I want to acknowledge the important role of my family, and specifically my parents, had on my development. Thank you for being so supportive, comprehensive and constantly encouraging me throughout my academic path and my life.

To the friends I've made during my academic life, thank you for the great moments and memories. Special thanks to the "Ayy Maria" group for all the support, good times and the friendship we shared throughout the years. To my oldest friends thank you for the continuous support and strong friendship. This endeavor would not have been possible without Mariana, thank you for always being there for me, always believing in me and for the kindness you gave me.

Palavras Chave GPP, NPP, Recuperação da Vegetação, Secas, Incêndios

Resumo

Eventos extremos como incêndios e secas afectam profundamente o ciclo global do carbono, uma vez que provocam degradação da vegetação. Por isso, uma monitorização global e contínua da dinâmica da vegetação é essencial para analisar os impactos desses eventos na vegetação e para compreender como esta recupera após fortes perturbações. A detecção remota fornece informação com uma ampla cobertura, alta resolução espacial e temporal, sendo por isso uma valiosa fonte de dados para estes estudos. Utilizando este tipo de dados, um estudo sobre a evolução da vegetação na Peninsula hibérica durante os últimos 21 anos é apresentado, onde é dada especial atenção a alguns incêndios que ocorreram em Portugal

Primeiro, foi feito um estudo climatológico da Península Ibérica utilizando dados MODIS MOD17A3 NPP. A análise dos mapas anuais e interanuais médios de NPP evidenciou as áreas mais produtivas. Uma análise de *clusters*, utilizando o método *k-means* sobre a variabilidade inter-anual do NPP, permitiu a discriminação de 5 regiões com características de vegetação distintas. Os valores de NPP de 3 *clusters*, localizados nas partes nordeste e oriental da Península Ibérica, mostraram uma tendência positiva ao longo dos últimos 20 anos. Esta tendência positiva parece estar associada a alterações na área de cada cobertura terrestre presente nos *clusters*, como revelado pela análise dos dados MCD12Q1 *land cover Type 2*. Foram também analisadas as séries temporais de NPP sobre Portugal e sobre quatro regiões (Norte, Centro, Alentejo e Algarve), bem como a evolução da cobertura terrestre nas mesmas zonas. Além disso, em Portugal observou-se uma diminuição de *Evergreen Needleaf Forests* e um aumento das *Graslands*. Por volta de 2017 observou-se uma diminuição acentuada do NPP em Portugal associado a *Evergreen Needleaf Forests* e um aumento acentuado do NPP associado a *Graslands*. Estas alterações pareciam ser coerentes com a severa época de incêndios florestais de 2017. Contudo, aquando da análise por região, foram obtidos resultados semelhantes em todas. Isto sugere que deveriam ser incluídos mais factores para explicar as alterações identificadas.

Para estimar os tempos de recuperação da vegetação no pós-fogo, foi aplicado um modelo que descreve anomalias de decaimento exponenciais, previamente aplicado a dados NDVI, aos dados MOD17A2 GPP, que têm maior resolução temporal. Os resultados obtidos para a área queimada de Monchique em 2003 são coerentes com os valores anteriormente obtidos quando o modelo foi aplicado aos dados NDVI. A aplicação do modelo à área ardida dos incêndios mais recentes de 2017 estima um tempo de recuperação de 39 meses para toda a área ardida em outubro desse ano. Quando o tempo de recuperação da produtividade da vegetação foi estimado em função do tipo de vegetação presente antes do incêndio, as áreas anteriormente ocupadas pelas *Savannas* mostram uma recuperação mais rápida (37 meses) da produtividade da vegetação do que as áreas anteriormente ocupadas por *Evergreen Needleaf Forests* (45 meses). Portanto, se o tempo de recuperação for estimado para diferentes subáreas da área ardida global, os seus valores podem ser diferentes devido às combinações de cobertura do solo presentes em cada sub-área. Isto foi verificado aplicando o modelo a duas sub-áreas da área ardida no centro de Portugal em outubro de 2017.

Keywords GPP, NPP, Vegetation recovery, Droughts, Wildfires

Abstract

Extreme events such as wildfires and droughts deeply affect the global carbon cycle, since they cause massive degradation of the vegetation greenness. A global and continuous monitoring of vegetation dynamics is essential to analyse the impacts of such events in the vegetation and to understand how it recovers after strong disruptions. Remote Sensing provides information with a wide coverage, high spatial and temporal resolution, being therefore a valuable source of data for these studies. Using this type of data, we present here a study of the vegetation evolution in the Iberian Peninsula during the last 21 years, and give special attention to some large wildfires that occurred in Portugal.

First, a climatological study of the Iberian Peninsula was done using MODIS MOD17A3 NPP data. The analysis of yearly and inter-annual mean NPP maps makes clear the areas with more vegetation productivity. A clustering analysis, using the k-means method on the inter-annual NPP variability, allowed the discrimination of 5 regions with distinct vegetation characteristics. The NPP integrated over 3 clusters, located in the northeastern and eastern parts of the Iberian Peninsula, showed a positive trend over the last 20 years. This seems to be associated with changes of the area of each land cover present in the clusters, as revealed by the analysis of the data in the MODIS MCD12Q1 land cover Type 2 product.

The integrated NPP time series over Portugal's mainland and over 4 regions (North, Central, Alentejo and Algarve regions) as well as the evolution of the land covers in the same areas were also analysed. Moreover, Portugal showed a decrease in Evergreen Needleleaf Forests and an increase in Grasslands were observed. A steep decrease in the integrated NPP over Portugal and associated with Evergreen Needleleaf Forest and an accentuated increase of the integrated NPP associated with Grassland were observed around 2017. These changes seemed to be coherent with the severe wildfire season of 2017. However, when the analysis was performed in each region, similar results were obtained in the North, Central, Alentejo and Algarve regions. This suggests more factors should be included to explain the identified changes.

To estimate recovery times post-fire, a model that describe exponential decaying anomalies, which was previously applied to NDVI data, was here applied to the more time resolved GPP data from the MODIS MOD17A2 product. The results obtained for the burnt area of Monchique in 2003 are coherent with the values previously obtained when the model was applied to NDVI data. The application of the model to the burnt area of the more recent wildfires of 2017 estimates a recovery time of 39 months for the whole burnt area by the wildfires in October of 2017. When the recovery time of vegetation productivity was estimated as a function of the vegetation type that was present before the wildfire, the areas previously occupied by Savannas show a faster recovery (37 months) of vegetation productivity than the areas that were previously occupied by Evergreen Needleleaf Forests (45 months). Therefore, if the recovery time is estimated for different subareas of the global burnt area their values may differ because the land cover combinations for each subarea may be different. This was verified by applying the model to two subareas of the burnt area in the centre of Portugal in October 2017.

Contents

List of Figures

List of Tables

List of Acronyms

CO_2	Carbon dioxide
MODIS	Moderate Resolution Imaging Spectroradiometer
NDVI	Normalized Difference Vegetation Index
NIR	near-infrared wavelength
RED	red wavelength
GPP	Gross Primary Production
NPP	Net Primary Production
R_a	Autotrophic Respiration
FPAR	Fraction of Photosynthetically Active Radiation
LAI	Leaf Area Index
T	Temperature
SWRad	Incident Shortwave Radiation
VPD	Vapour Pressure Deficit
BPLUT	Biome Parameter Lookup Table
ε	Radiation Conversion Efficiency
IPAR	Incident Photosynthetically Active Radiation
APAR	Absorbed Photosynthetically Active Radiation
SLA	Specific Leaf Area
R_{ml}	Maintenance Respiration of Leaves
R_{mfr}	Maintenance Respiration of Fine Roots
PSN_{net}	Daily Net Photosynthesis
R_{mlw}	Maintenance Respiration Costs of Live Wood
R_g	Annual Growth Respiration Costs
R_m	Annual Plant Respiration Cost
AppEEARS	Application for Extracting and Exploring Ready Samples

UMD	University of Maryland classification scheme
ENF	Evergreen Needleleaf Forest
EBF	Evergreen Broadleaf Forest
CS	Closed Shrublands
OS	Open Shrublands
WSV	Woody Savannas
SV	Savannas
GS	Grasslands
CP	Croplands
STD	Standard Deviation
SSED	Sum of Squared Euclidian Distances
CNE	Cluster North-Eastern
CE	Cluster Eastern
CSW	Cluster South-Western
CNW	Cluster North-Western
CC	Cluster Central
GY	Gorgeous Year

1

Introduction

The vegetation dynamics is very sensitive to climatic changes. Small variations in temperature and water availability can impact vegetation quantity and growth (Roerink et al., 2003; Gouveia et al., 2009, 2012; Wu et al., 2015). These factors negatively affect plant respiration, evapotranspiration, and photosynthesis, leading to a decreased uptake of atmospheric CO_2. Some of the resulting atmospheric CO_2 increase is compensated by the uptake by other natural sinks involved in the global carbon cycle (Figure 1.1). On top of the natural carbon cycle, anthropogenic emissions cause an imbalance in this cycle (Figure 1.1). The most notable sources of these emissions are fossil fuel combustion and land-use change. The latter is associated with deforestation that directly impacts vegetation quantity (Friedlingstein et al., 2022).

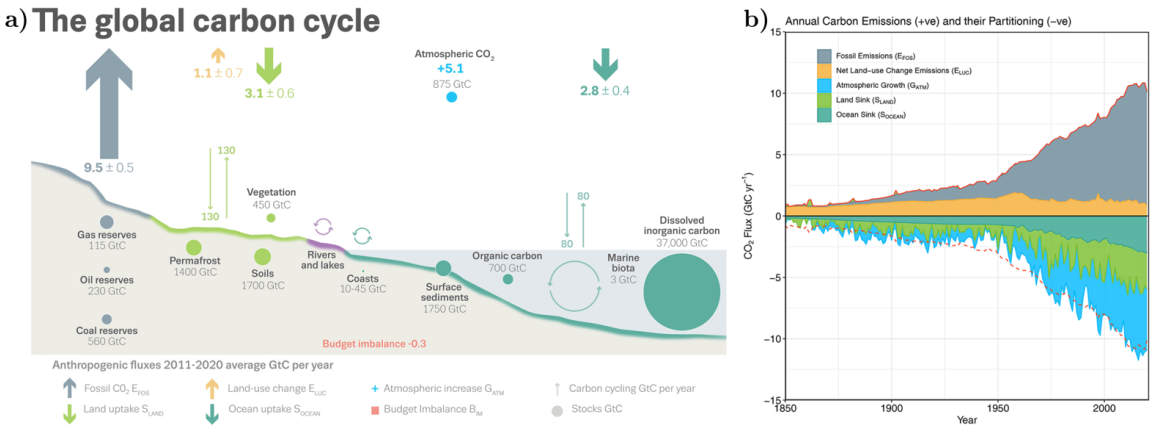

Figure 1.1: Schematic representation of the global carbon cycle perturbations (a), represented over time (b). Adapted from Friedlingstein et al. (2022)

In addition, vegetation biomass combustion also reduces terrestrial biomass and influences vegetation patterns. Inevitably, there is a loss in carbon stored on land, as

well as emissions of other greenhouse gases and aerosols (Bond et al., 2005; Ward et al., 2012; Voulgarakis and Field, 2015; Friedlingstein et al., 2022).

Extreme events like heatwaves, droughts, frosts, heavy precipitation, or heavy storms are also associated with disturbances in the carbon sinks that can even be responsible for the reductions in the carbon stocks, and therefore, increasing the atmospheric CO_2 (Reichstein et al., 2013; Frank et al., 2015). All these impacts can be felt instantly but also present a lagged effect that impacts the affected area in the coming years (Wu et al., 2015). Many authors pointed that, out of all the extreme events, drought presents the most widespread and strongest consequences in the carbon cycle (Zavalloni et al., 2008; Gilgen and Buchmann, 2009; van der Molen et al., 2011; Reichstein et al., 2013; Frank et al., 2015). In particular, the Iberian Peninsula has been affected by very severe droughts throughout the times. One outstanding example is the 2004/2005 drought. In this event, only 40% of the usual amount of water precipitated, marking the driest event in the 140 years preceding it (García-Herrera et al., 2007).

Since the Mediterranean climatic zones house roughly 20% of the world's flora and a wide variety of species, extreme events like wildfires in these zones are a cause for concern since some species are not able to survive (Cowling et al., 1996; Retana et al., 2002; Lloret and Vilà, 2003; Bastos et al., 2011). The severity and occurrence of wildfires are often associated with some climatic variables, such as high temperatures, lack of precipitation, wind, and others that also strongly influence fauna and flora conditions.

During the post-fire period, the vegetation goes through a slow recovery and usually before fully recovering to what it was before the fire, transitional vegetation grows in the area. This type of vegetation grows rapidly with the availability of water and may dry and/or die very quickly, giving place to persistent vegetation. This new vegetation is not always the same as it was before the event, as new species may vegetate the affected area (Retana et al., 2002; Lloret and Vilà, 2003). To monitor the extent of extreme events, such as wildfires, the recovery of vegetation patterns, and the effects on the global CO_2 balance, there is a need for a truly global method of analysis (Exbrayat et al., 2019), easily achieved using remote sensing information.

The data used for vegetation studies are derived from radiation in spectral bands with different sensitivities to the biogeochemical photosynthetic processes in the leaves (Jacquemoud and Baret, 1990; Myneni et al., 1995). The reflected solar radiation is measured at some specific wavelengths, being the broad-band red (0.6-0.7 µm) and the near-infrared (0.75 -1.35 µm) the most important for vegetation studies. Over the years many satellites were launched and with each new iteration more and better sensors were packed onto them. Examples of the use of such sensors are the ESA's (European Space Agency) PROBA (PRoject for OnBoard Autonomy; Hagolle et al., 2005; ESA, 2022a,b) and SPOT (Satellite pour l'Observation de la Terre; ESA, 2018, 2022c) missions and

the NASA's (National Aeronautics and Space Administration) Moderate Resolution Imaging Spectroradiometer (MODIS; NASA, 2022) program, aboard two satellites, Terra and Aqua. With the technological improvements nowadays, these sensors can provide products with 1 km to 100 m resolution.

The so-called Vegetation Indexes (VI) are of the first products derived using information from sensors on board satellites. They continue to be widely regarded as one of the best ways to monitor the quantity and role of terrestrial vegetation at a global level (Zhou et al., 2001; Lucht et al., 2002; Nemani et al., 2003; Xue and Su, 2017; Giovos et al., 2021). Among these indexes, the Normalized Difference Vegetation Index (NDVI) stands out. It was proposed in first time by Rouse Jr et al. (1974), and it is defined as the difference in near-infrared (NIR) and red wavelengths (RED) surface reflectance values, normalized over the sum of these values.

With the increasing importance of monitoring the carbon cycle and other problems like deforestation, the Gross Primary Production (GPP) and the Net Primary Production (NPP) gained popularity in the scientific community. The first is defined as the daily total rate of photosynthesis, or in order words, the rate of carbon uptake through photosynthesis, while the latter reflects the annual integrated GPP minus the annual value of carbon rate produced by plant respiration (Running et al., 2000, 2004). These two products are connected as GPP represents the total rate of carbon uptake and NPP the net rate of carbon stored by vegetation. In other words, NPP is GPP without respiration costs, as schematized in Figures 1.2 and 1.3. These indexes will be used in this work and will be detailed further ahead.

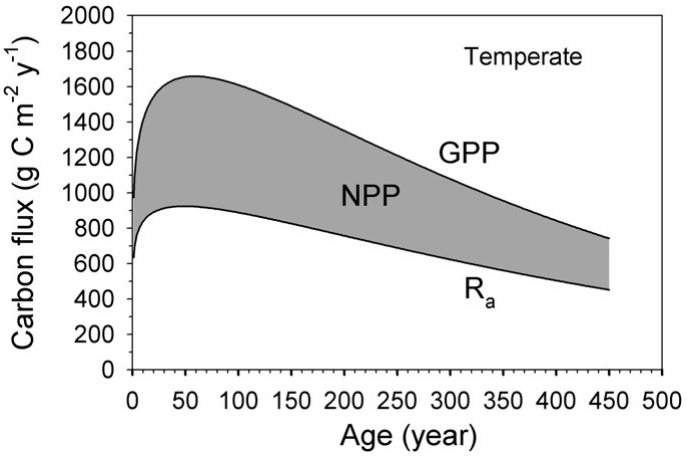

Figure 1.2: GPP and Autotrophic Respiration Cost (R_a) curves and the difference between the two (NPP) represented for a temperate forest. Adapted from Tang et al. (2014).

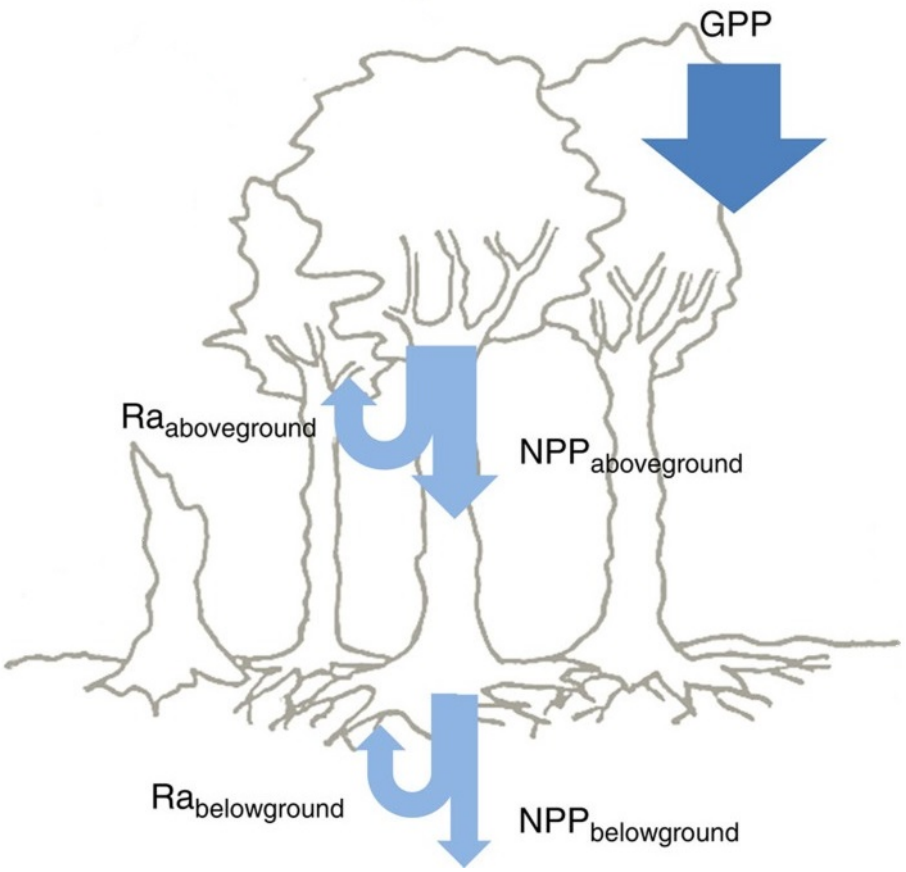

Figure 1.3: Schematic representation of the major components of the carbon balance in the vegetation. R_a, in Figure 1.2, is the sum of $R_{a\ aboveground}$ and $R_{a\ belowground}$, and the total NPP is calculated by subtracting the R_a from the GPP values. Arrows pointing down represent carbon uptake, while arrows pointing up indicate a carbon release. (Adapted from Campioli et al. (2016))

The aforementioned products can be used as input for vegetation modelling. Several studies used remotely sensed data to assess vegetation growth after extreme events, such as fire (Marchetti et al., 1995; Viedma et al., 1997; Díaz-Delgado et al., 1998; Díaz-Delgado and Pons, 2001; Díaz-Delgado et al., 2002; Úbeda et al., 2006; Röder et al., 2008; Gouveia et al., 2010). The work of Gouveia et al. (2010) proposed a mono-parametric relaxation model to estimate the recovery times for the vegetation using SPOT/VEGETATION data at 1 km spatial resolution. Bastos et al. (2011) applied the same model as Gouveia et al. (2010) on a lengthier dataset to assess the model's accuracy, its sensitivity to initial conditions, analysing two large wildfire events. Their study was based on monthly values of NDVI over 11 years (1998-2009). It was deemed that the methodology proposed by Gouveia et al. (2010) was adequate to estimate recovery times. Also, it was noted that the fact that the model relies solely on one parameter makes the process of assessing recovery times a simple task (Bastos et al., 2011). Gouveia et al. (2018) revisited the model, with MODIS data at 500m

spatial resolution, in order to assess its consistency and robustness. They argued that the model was adequate for the study of post-vegetation dynamics, and it will help plan better policies for fire prevention, management, and eventual mitigation. The authors also indicate that the modelled recovery times are sensitive to the impact of drought events on the pre- and post-fire vegetation dynamics (Bastos et al., 2011; Gouveia et al., 2012).

The present work aims to analyse how the Iberian vegetation responds to wildfires and drought events, using GPP and NPP datasets with a higher time resolution than that used in the previous works by Bastos et al. (2011) and Gouveia et al. (2010, 2012, 2018). A climatological study of the NPP time series was made in order to characterise the vegetation patterns and tendencies and to better understand how some extreme events impact the development of the vegetation. Then, Gouveia's model was modified to be applied with GPP data from MODIS program. This was made to assess the sensitivity of the model to the use of a different vegetation index (remember that the previous studies used the NDVI index), and to assess the effect of time resolution of the data on a more precise definition of the initial conditions.

2

Data and Methods

2.1 Biophysical Data Derived from Satellite Observations

As was noted in the previous chapter, GPP and NPP remote sensing data play an important role in vegetation studies. The datasets used in this work were obtained from the MODIS sensor, which is carried aboard of, both, Terra and Aqua satellites since 2000 and 2002, respectively, until now. The algorithm used to calculate the GPP and NPP will be detailed in the next subsection.

2.1.1 MODIS GPP/NPP Algorithm

The MODIS MOD17A2/A3 GPP and NPP algorithm is based on the light use efficiency approach first proposed by Monteith (1972). The algorithm requires several inputs to compute GPP and NPP (Figure 2.1). Information about vegetation is derived from the Fraction of Photosynthetically Active Radiation (FPAR) absorbed by green vegetation and is obtained from the MODIS MOD15A2H product which also includes the Leaf Area Index (LAI, in m^2 leaf per m^2 ground area) values. Both FPAR and LAI products are derived from the spectral information of the MODIS RED (648 nm) and NIR (858 nm) surface reflectance. If, for some reason, this cannot be done, the values are derived with a backup algorithm based on the relation between NDVI and FPAR or LAI, respectively (Myneni, 2020). The algorithm also requires data from Temperature (T, in °C), incoming solar radiation (also known as incident shortwave radiation (SW Rad, in $MJ \cdot m^{-2}$ in 3-h periods), and Vapour Pressure Deficit (VPD, in Pa) that are derived from meteorological reanalysis, more specifically the NASA's Global Modelling and Assimilation Office (GMAO) and the National Centres for Environmental Prediction and the National Centre for Atmospheric Research (NCEP/NPAR) joint Reanalysis (Zhao et al., 2005, 2006).

An essential input of the algorithm is the Land Cover classification. The most recent version of the algorithm uses the Land Cover Product MCDLCHKM, which employs the University of Maryland land cover classification scheme (Sulla-Menashe and Friedl, 2018; Running and Zhao, 2019). Other essential element of the algorithm is the Biome Parameter Lookup Table (BPLUT) which prescribes the values of maximum radiation conversion efficiency (ε_{max}, in kg C MJ^{-1}), the parameters for T and VPD limits, specific leaf area and respiration coefficients for each land cover type (Running et al., 2000).

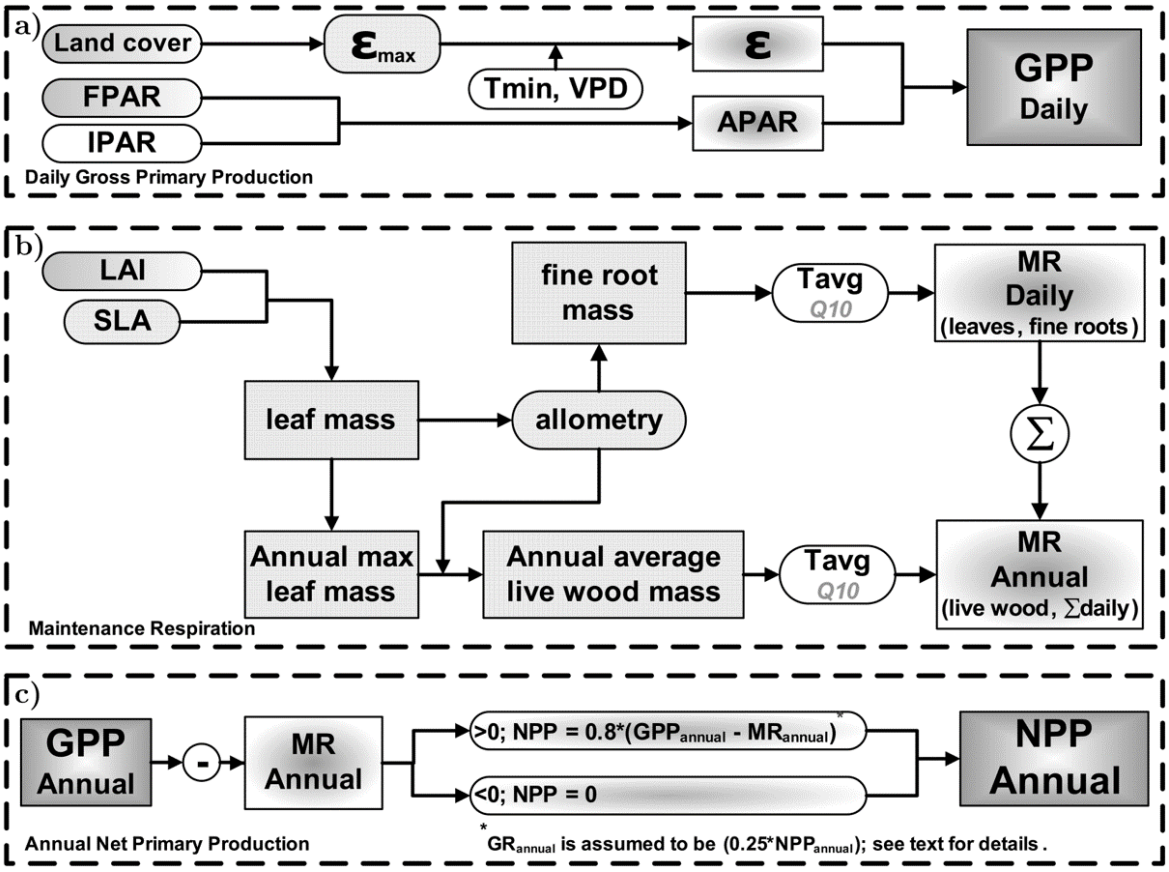

Figure 2.1: Flowcharts representing the GPP/NPP algorithm. a) Module used to calculate the daily GPP. b) Module used to calculate the daily and annual respiration costs. c) NPP Algorithm based on the previous two modules. (Adapted from Running and Zhao (2019))

With these input datasets, GPP can be computed (Figure 2.1a). First, the Incident Photosynthetically Active Radiation ($IPAR$) is estimated from the $SWRad$ as:

$$IPAR = SWRad \times 0.45 \tag{2.1}$$

The Absorbed Photosynthetically Active Radiation ($APAR$) can be calculated by multiplying $FPAR$ by $IPAR$. A direct estimation of the $FPAR$ is available from

the $NDVI$ data as $FPAR \approx NDVI$. Therefore, the $APAR$ can be estimated by the following equation

$$APAR = FPAR \times IPAR \approx NDVI \times IPAR \tag{2.2}$$

The radiation conversion efficiency (ε) varies according to the type of vegetation (Field et al., 1995; Turner et al., 2003; Kemanian et al., 2004) and non-ideal climate conditions also affect the photosynthetic capabilities of vegetation (RAYMOND HUNT JR, 1994; Turner et al., 2003; Running et al., 2004; Running and Zhao, 2019). Due to this, the ε_{max}, obtained from the BPLUT, must be attenuated by the daily minimum temperature (T_{min}, in °C) and by the daylight averaged vapour pressure deficit (VPD, in Pa). Applying these control factors, an effective radiation conversion efficiency, ε (in kg C MJ^{-1}), is obtained. Using the estimated ε and the $APAR$, the GPP (in kg C m^{-2} day^{-1}) can be calculated as:

$$GPP = \varepsilon \times APAR \tag{2.3}$$

The GPP calculated on a daily basis is made available as an 8-day product. This makes for forty-six composites per year, where the first forty-five composites represent 8 days and the last represents five (or six in a leap year) days. The date of each 8-day composite corresponds to the first day of each 8-day period.

Besides GPP, maintenance respiration costs are also calculated daily, and a brief scheme of their calculation is shown in Figure 2.1b). The calculations use the LAI dataset alongside daily averaged temperature (T_{avg}, in °C), obtained from the meteorology dataset, and five parameters read in the BPLUT. These are specific leaf area (SLA, in m^{-2} kg C), the ratio between fine root and leaf, maintenance respiration values for leaf and fine root per day at 20°C ($leaf\_mr\_base$ and $froot\_mr\_base$, respectively, both in kg C kg C^{-1} day^{-1}), and a temperature-dependent exponential parameter that regulates respiration (Q_{10}, dimensionless).

The leaf mass (in kg) is obtained by dividing LAI by SLA. Then, the fine root mass (in kg) is calculated by multiplying the leaf mass by the fine root to leaf ratio. From here the maintenance respirations can be calculated for both the leaf (R_{ml}, in kg C day^{-1}) and fine root (R_{mfr}, in kg C day^{-1}). The following equations are used

$$R_{ml} = Leaf_{Mass} \times leaf\_mr\_base \times Q_{10}^{\left[\frac{T_{avg}-20}{10}\right]} \tag{2.4}$$

$$R_{mfr} = Leaf_{Mass} \times froot\_mr\_base \times Q_{10}^{\left[\frac{T_{avg}-20}{10}\right]} \tag{2.5}$$

With the maintenance respiration costs of leaves and fine roots calculated, the daily net photosynthesis (PSN_{net}, in kg C day^{-1}) can be obtained from the daily GPP values as:

$$PSN_{net} = GPP - R_{ml} - R_{mfr} \tag{2.6}$$

Like the GPP, the PSN^{net} is summed over 8-day periods. This product still does not consider the annual maintenance respiration costs of live wood (R_{mlw}, in kg C) nor the annual growth respiration costs (R_g, in kg C). The first of these two can be calculated much like maintenance respiration for leaves and fine roots, only changing the inputs from leaf or fine root to their live wood counterparts. The second, as suggested by (Ryan, 1991), is empirically estimated to be 25% of NPP. This was made to improve the algorithm as the R_g derived from the LAI sometimes caused these values to be so high that negative NPP values were obtained. With all the above parameters calculated, NPP (Figure 2.1c) can be written as such:

$$NPP = \sum_{i=1}^{365} PSN_{net} - (R_{mlw} + R_g) \simeq \sum_{i=1}^{365} GPP - R_m - 0.25 \times NPP \tag{2.7}$$

where R_m is the annual plant respiration cost and is calculated in the following way:

$$R_m = \sum_{i=1}^{365} R_{ml} + \sum_{i=1}^{365} R_{mfr} + R_{mlw} \tag{2.8}$$

Equation 2.7 can be simplified and defined by branches. Resulting in equation 2.9, which represents the calculus done by the algorithm to obtain the NPP (in kg C m^{-2}).

$$NPP = \begin{cases} 0.8 \times \left(\sum_{i=1}^{365} GPP - R_m\right) & \sum_{i=1}^{365} GPP - R_m \geq 0 \\ 0 & \sum_{i=1}^{365} GPP - R_m < 0 \end{cases} \tag{2.9}$$

2.2 Datasets and Specification

2.2.1 NPP and GPP

The NPP and GPP data from the products MODIS MOD17A3 and MOD17A2 were downloaded from NASA's Application for Extracting and Exploring Ready Samples (AppEEARS, 2022). These products are available globally from 2000 until the present at a 500 m spatial resolution and are produced in sinusoidal coordinates and later converted to the geographic coordinates, as used here. This study is focused on twenty-year period (2001-2020) over the Iberia region. In order to have a longer period of data after the 2017 fire, that will be studied in chapter 3, the GPP data for 2021 was also downloaded, when it was made available. The interface to download the data allows the definition of

a rectangular window area as shown in Figure 2.2a). After defining the area of interest the data is downloaded in format NetCDF-4 for all land grid points included in the window as shown in 2.2b). As the objective of this study was to focus on the Iberian Peninsula some areas were masked. These areas include the south of France, all land belonging to Africa and the Balearic Islands. It should be noted that only thirty-three GPP composites are available during 2002.

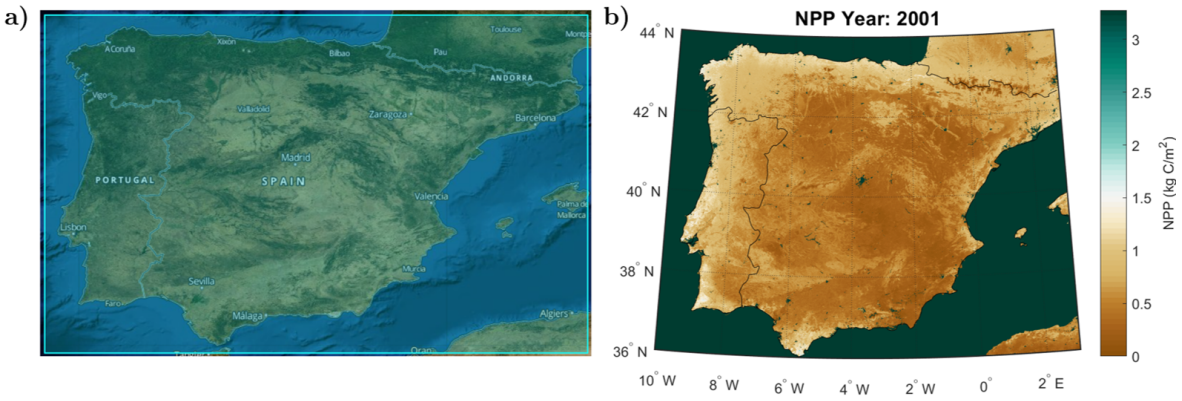

Figure 2.2: AppEEARS data selection window obtained from Leaflet NASA EOSDIS GIBS(a) and the raw NPP data represented over the Iberian Peninsula (b).

After the pre-processing of data mentioned above, the final maps obtained are in the form of the one represented in Figure 2.3.

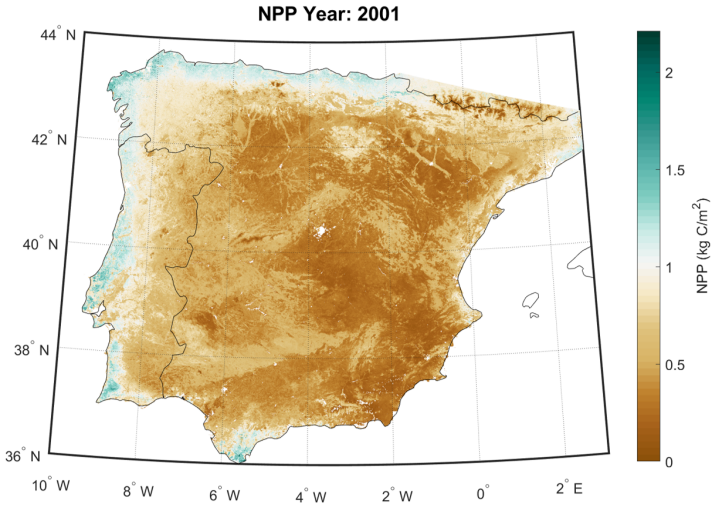

Figure 2.3: Representation of the MODIS NPP for the year 2001 after applying the pre-processing scheme.

The GPP data is available with a time resolution of 8 days, i.e., each GPP value represents the integrated value in the 8-day period following the day to which it is referred, except for the last value of each year, which corresponds to a value integrated over five (or six in a leap year) days. Therefore, for each grid point, we have 46 values

of GPP each year. In order to have all values normalized to the same time period, the 46th value in each year was rescaled for a period of eight days. This was achieved by multiplying the last value of each year by eight and dividing by five (or six in leap years).

2.2.2 Land Cover

The land cover dataset used in this work was the MODIS MCD12Q1 product downloaded from NASA's AppEEARS website, that corresponds to the land cover classification system developed at University of Maryland. It has a 500 m resolution and, like the other MODIS products, is produced in sinusoidal coordinates and later projected to the geographic coordinates used here. In order to be in agreement with the GPP/NPP data, this dataset was extracted for the years 2001 to 2019 (the 2020 map was not available at the time of this work) and for the same area (36ºN to 44ºN and 10ºW to 3ºE). Furthermore, data from the south of France, North of Africa, and the Balearic Islands were removed so all the datasets would be in agreement. As an example, the Land Cover in 2001 is shown in Figure 2.4.

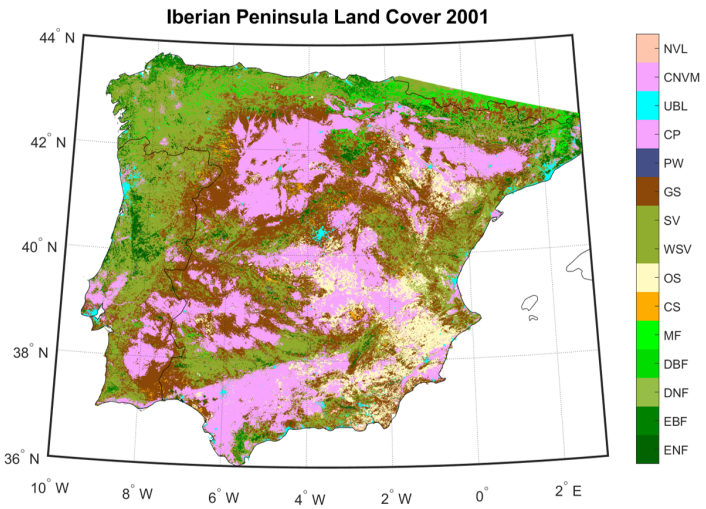

Figure 2.4: Land Cover types displayed in the Iberian Peninsula (2001).

The MODIS Land Cover Type (MCD12Q1) product is calculated from supervised reflectance data classifications obtained by the Terra and Aqua satellites. This product is generated yearly with a 500-meter grid and has five land cover classification schemes. These are the International Geosphere-Biosphere Programme land cover classification (IGBP; Loveland and Belward (1997)), the University of Maryland classification scheme (UMD; Hansen et al. (2000)), the LAI/FPAR Biome classification scheme (LAI;Myneni et al. (2002)), the Biome-Biogeochemical Cycles classification scheme (BGC; Running et al. (2004)) and the Plant Functional Type classification scheme (PFT; Bonan et al. (2002)). These classification schemes are referred to LC_Type1, LC_Type2, LC_Type3,

LC_Type4, and LC_Type5 respectively. In this study, we will use the LC_Type2 scheme, which refers to the same UMD classification used in the MODIS MOD17A2/A3 algorithm (Running and Zhao, 2019). This scheme has eleven natural vegetation classes, three human-altered classes and two non-vegetated classes, totalling for sixteen classes. Specifications on each vegetation type can be found in Table 2.1, obtained from the MODIS Land Cover User Guide (Sulla-Menashe and Friedl, 2018).

2.2.3 Burnt Areas

The Pixel Burned Areas[†] product from the MODIS Burned Areas FireCCI version 5.1 (FireCCI51) was used to identify fire scars across the Iberian Peninsula. Therefore, data for the years 2003, 2005, 2012 and 2017 were downloaded as, in these years, massive fires occurred across Portugal and Spain.

The FireCCI51 algorithm produces maps of global burnt areas for the period 2001-2020. This was preceded by the MERIS FireCCI version 4.1 (FIRECCI41; Chuvieco et al. (2016)) which ranged from 2005 to 2011, and the MODIS FireCCI version 5.0 (FireCCI50; Chuvieco et al. (2018)) which covered the period from 2001 to 2016. This algorithm needs the input of the MOD09GQ Collection imagery, which contains daily surface reflectance in the RED and NIR bands with 250 m spatial resolution. Additionally, these reflectances are combined with the MOD09GA Collection 6 product, and the quality of the data can be assessed.

The dates of occurrence of wildfires were obtained from the Pixel Burned Area product. This product has three layers which contain the date of detection, the confidence level and the land cover in the pixel that burnt. The layer containing the dates of wildfire occurrence comes in Julian Days (ranging from 1-366) and for unburnt cells, missing data, and water bodies the value is zero. Note that the date could not be always registered at the exact day the fire started as the "route" of the satellite, clouds, aerosols, and "thick" smoke may prevent fire detection (Lizundia-Loiola et al., 2020).

[†]Here we used the American English spelling (burned) to give names of products exactly as they are provided.

Table 2.1: University of Maryland classification scheme and class definitions. The Value column refers to the the number given in the code for each individual land cover (Adapted from Sulla-Menashe and Friedl (2018)).

Name	Acronym	Value	Description
Water Bodies		0	At least 60% of area is covered by permanent wa ter bodies.
Evergreen Needleleaf Forests	ENF	1	Dominated by evergreen conifer trees (canopy >2m). Tree cover >60%.
Evergreen Broadleaf Forests	EBF	2	Dominated by evergreen broadleaf and palmate trees (canopy >2m). Tree cover >60%.
Deciduous Needleleaf Forests	DNF	3	Dominated by deciduous needleleaf (larch) trees (canopy >2m). Tree cover >60%.
Deciduous Broadleaf Forests	DBF	4	Dominated by deciduous broadleaf trees (canopy >2m). Tree cover >60%.
Mixed Forests	MF	5	Dominated by neither deciduous nor evergreen (40-60% of each) tree type (canopy >2m). Tree cover >60%.
Closed Shrublands	CS	6	Dominated by woody perennials (1-2m height) >60% cover.
Open Shrublands	OS	7	Dominated by woody perennials (1-2m height) 10-60% cover.
Woody Savannas	WSV	8	Tree cover 30-60% (canopy >2m).
Savannas	SV	9	Tree cover 10-30% (canopy >2m).
Grasslands	GS	10	Dominated by herbaceous annuals (<2m).
Permanent Wetlands	PW	11	Permanently inundated lands with 30-60% water cover and >10% vegetated cover.
Croplands	CP	12	At least 60% of area is cultivated cropland.
Urban and Built-up Lands	UBL	13	At least 30% impervious surface area including building materials, asphalt, and vehicles.
Cropland/Natural Veget. Mosaics	CNVM	14	Mosaics of small-scale cultivation 40-60% with natural tree, shrub, or herbaceous vegetation.
Non-Vegetated Lands	NVL	15	At least 60% of area is non-vegetated barren (sand, rock, soil) or permanent snow and ice with less than 10% vegetation.
Unclassified		255	Has not received a map label because of missing inputs.

3

Results

In this chapter, the results are grouped in three subsections. In the first section, NPP values were used to make a climatological study, calculating their time mean and standard deviation, and trends. In the second section, the clustering technique k-means was used to identify vegetation patterns along the Iberian Peninsula. Moreover, with the land cover data, the NPP dataset was analysed by land cover type. Finally, the third section presents an analysis of vegetation recovery in Portuguese mainland areas that had shown higher susceptibility for the occurrence of severe wildfires. With the aforementioned datasets, the types and quantity of vegetation burnt each year were characterized.

3.1 Climatological analysis of NPP over the Iberian Peninsula

Figure 3.1 represents NPP for each of the 20 years of data available (2001-2020). In the graphs, it is possible to identify some burnt areas due to wildfires. This is most visible in 2003, 2005, 2012 and 2017. These burnt areas are possible to identify due to the steep change between the preceding year and the year when the wildfire occurred. One example of this is the Monchique area in 2002 had values of NPP of $2\,\mathrm{kg\,C/m^2}$, and in the year 2003, the same area had values of $1\,\mathrm{kg\,C/m^2}$. This implies a decrease of $1\,\mathrm{kg\,C/m^2}$ between 2002 and 2003, which indicates that there was an event that strongly affected NPP.

Areas with high NPP production and others that present low values of NPP are also evident in Figure 3.1. As expected, the Portuguese coastal regions (west Portugal and northwest Spain) have the highest NPP values. This higher vegetation productivity, as depicted by the higher NPP values, is associated with favourable climatic conditions over these areas. On the other hand, the regions in the centre of the Iberian Peninsula

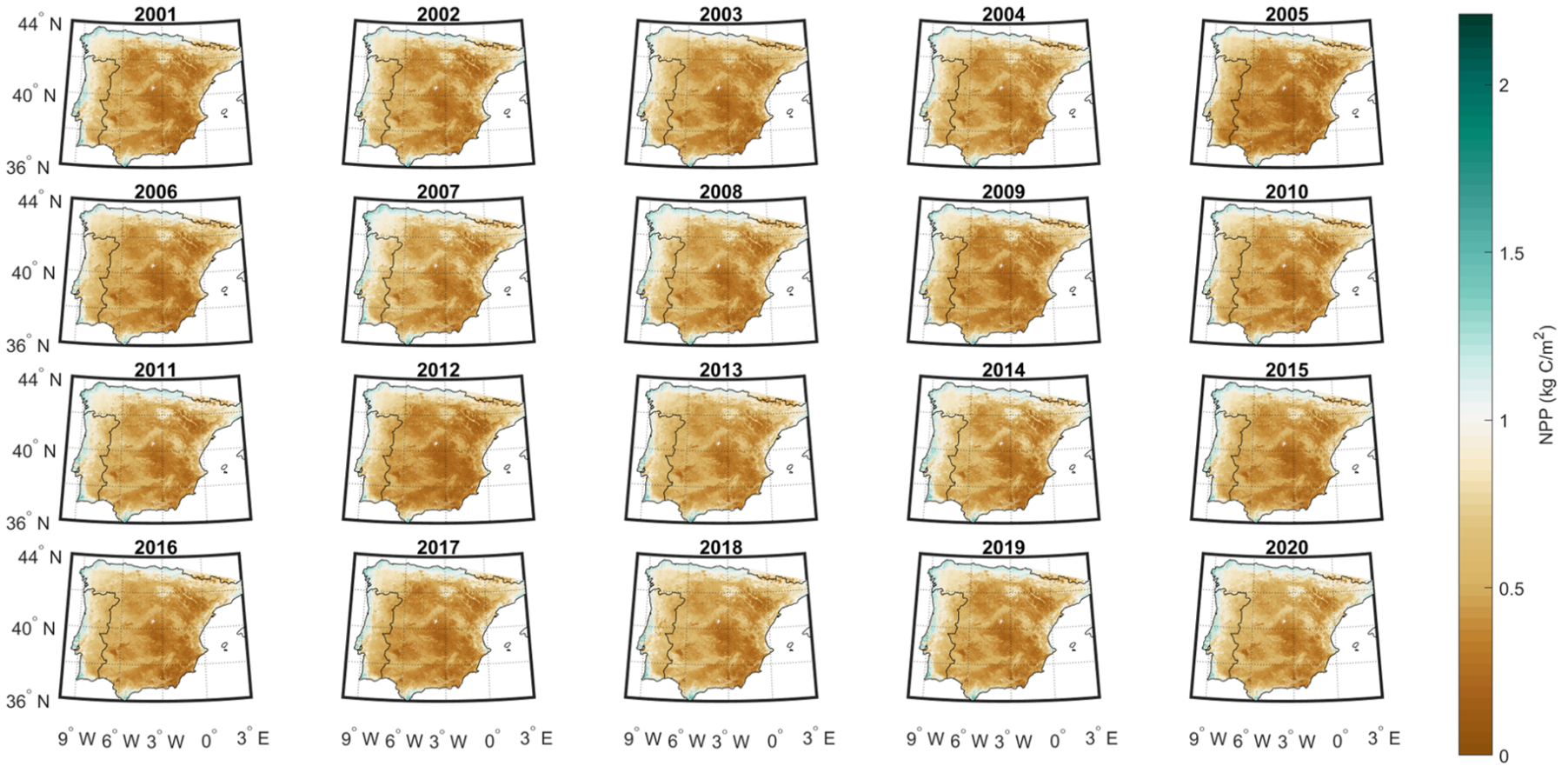

Figure 3.1: Annual variation of NPP for the Iberian Peninsula (2001-2020).

presented low NPP values, characteristics of less productive vegetation typically available over the semi-arid regions.

The mean and standard deviation (STD) across all the years is shown in Figure 3.2. In 3.2a) is again evident the higher NPP values located over Western and North-Western coast of the Iberian Peninsula, while the lowest values are located over Central and Eastern regions of the Iberia. In Figure 3.2b) the highest standard deviation values appear in areas that were affected by wildfires. The Monchique area, in the southwestern region of Portugal, has a high standard deviation value due to the recurrent occurrence of wildfires in that area (notably the 2003, 2004, 2016 and 2018 wildfires (ICNF, 2018)). Also, some of these high deviation values may be related to dam's constructions, as the Alqueva. These values would affect the study of the NPP variability associated with climate factors. Therefore, from visual inspection, a threshold of 0.11 kg C/m^2 was defined in order to select vegetated areas not affected by large wildfires and strong human induced changes. Because the high STD values are, presumably, due to large wildfires or drastic land use changes, such as the construction of large dams, the grid points where such STD values occur were not considered for the climatological analysis.

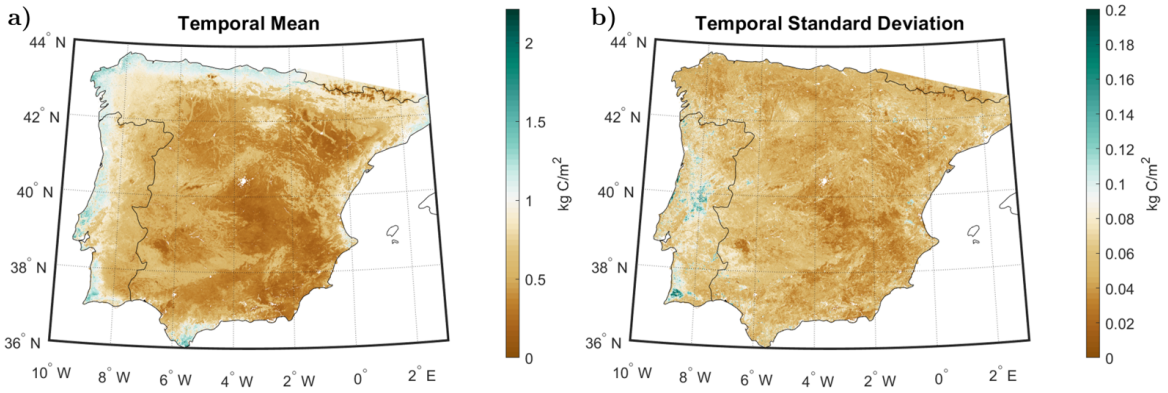

Figure 3.2: NPP Temporal Mean averaged over the Iberian Peninsula (a), where higher (green) values represent more productive pixels and lower (brown) values represent less productive pixels, and Standard Deviation (b), where higher (blue) values represent higher standard deviations and lower (brown) values represent pixels that have very little variation over time.

Figure 3.3 represents the linear trends for each pixel for the twenty-year period of 2001-2020, considering all points and only the points for which the STD is smaller than 0.11 kg C/m^2. Both images show that most of the trends are positive. In Figure 3.3a) it is possible to see that most of the deep red colours are from aquatic environments, such as the Guadiana River in the South of Portugal, and most of the deep blue colours relate to wildfires such as in the Monchique area and others. In Figure 3.3b) the deep colours are gone, because the points with STD higher than 0.11 kg C/m^2 were eliminated from the analysis by the reasons explained above.

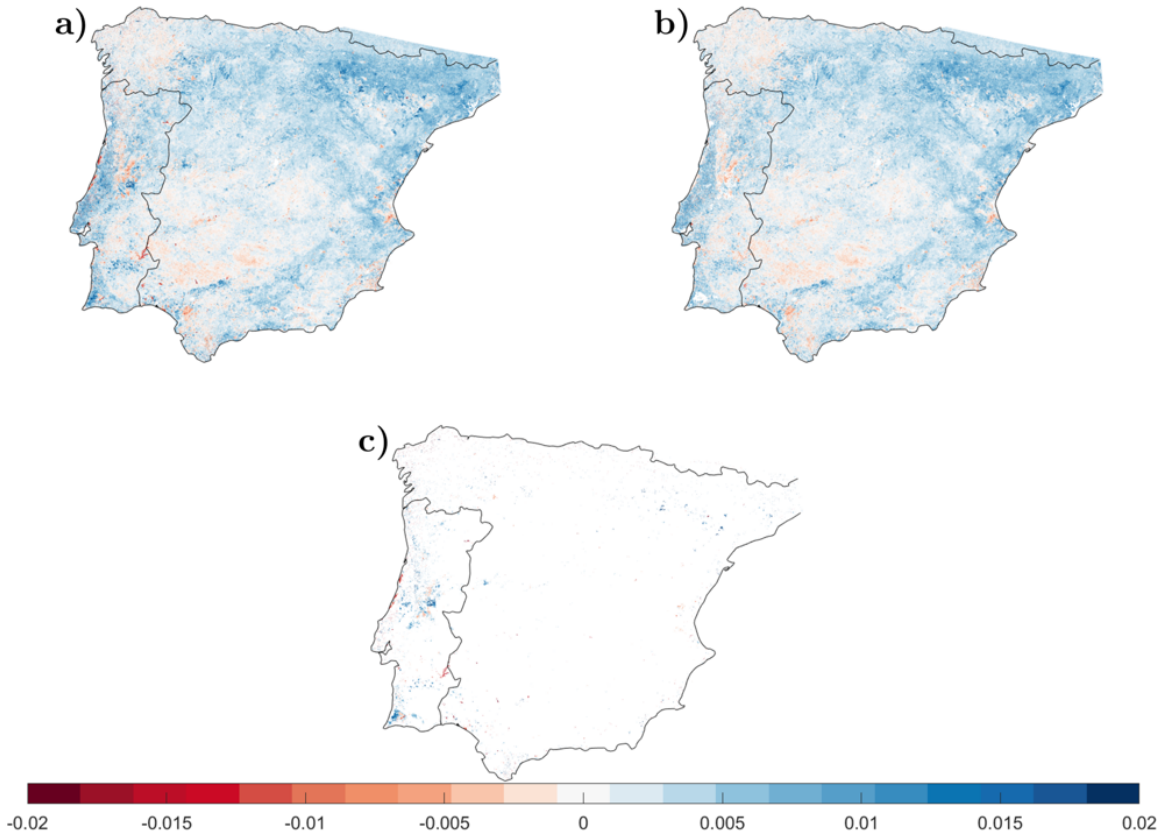

Figure 3.3: Trend for the 20 years, red zones have a negative trend and blue zones have a positive trend. (a) All values. (b) Values with a standard deviation lower than 0.11 kg C/m^2 (c) Values with a standard deviation higher than 0.11 kg C/m^2.

In order to study regional patterns of variability and trends, which may be associated with climate variables, a k-mean clustering analysis was applied to the NPP data. Before the application of the cluster analysis, the NPP time series were centred to have mean 0 and normalized by the respective standard deviations. Several numbers of clusters were tested, with the distances calculated as the Squared Euclidian Distance (SED) to the centroid of the respective clusters. Applying the k-mean clustering for different k values, we calculated the Sum of Squared Euclidean Distances (SSED). An indication of the better k value to be used in our analysis was obtained following the idea of the elbow method. Although a clear inflexion point, i.e. a point where the rate of decrease of the SSED stabilizes, can not be identified, we can see that the use of a value k=5 considers the steepest changes of the SSED (Figure 3.4; Sharma (1995)). Moreover, to better understand the differences between the different k values, the cluster technique was applied to various k values (k=3, k=4, k=5, k=6, k=7). From this analysis, values of k above 5 (k>5) showed the same general regions and very similar vegetative cycles to k=5. Values below 5 (k<5) showed too much variation within each cluster regarding the dominant vegetation covers. The value of k=5 represents reasonably coherent geographic areas (see Figure. 3.5).

Clusters are designed according to the regions where they are predominant (Figure 3.5a). Table 3.1 gives the abbreviations to be used in the text.

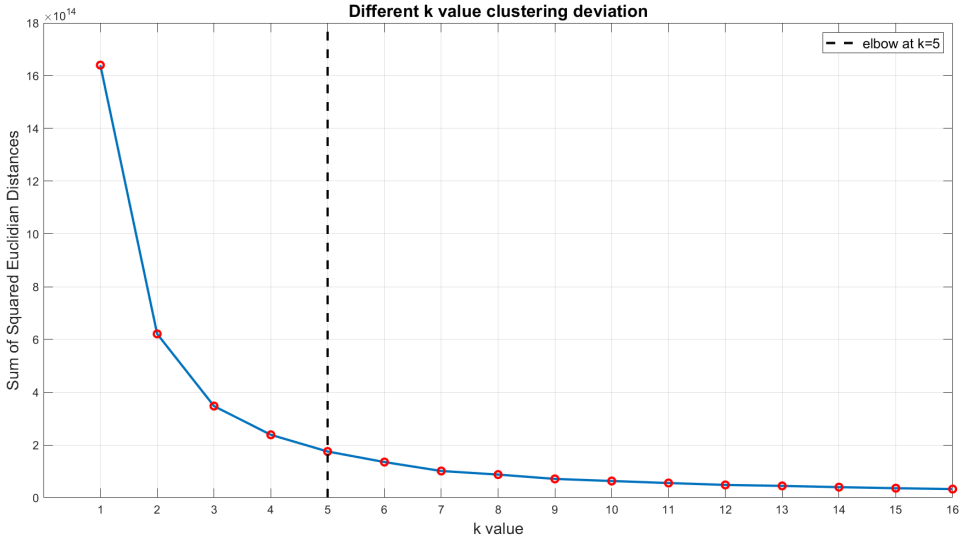

Figure 3.4: Elbow method for evaluating clusters. Sum of Squared Euclidian Distances for each k value.

Table 3.1: Cluster names, location and abbreviation that will be used in the following analysis.

Cluster	Location	Abbreviation
1	North-Eastern	CNE
2	Eastern	CE
3	South-Western	CSW
4	North-Western	CNW
5	Central	CC

Cluster CNE is predominant in the North/North-Eastern part of Spain and cluster CE is distributed along the Eastern coast of Spain. Cluster CSW includes Central and South Portugal as well as the Western Central and South of Spain, whereas cluster CNW is majorly located in the North of Portugal and the North-Western part of Spain. Lastly, cluster CC is predominant in the Central North of the Iberian Peninsula, along the coast of the Central Region of Portugal. Additionally, some dispersed patches of the cluster CC are also found in the South of the Iberian Peninsula.

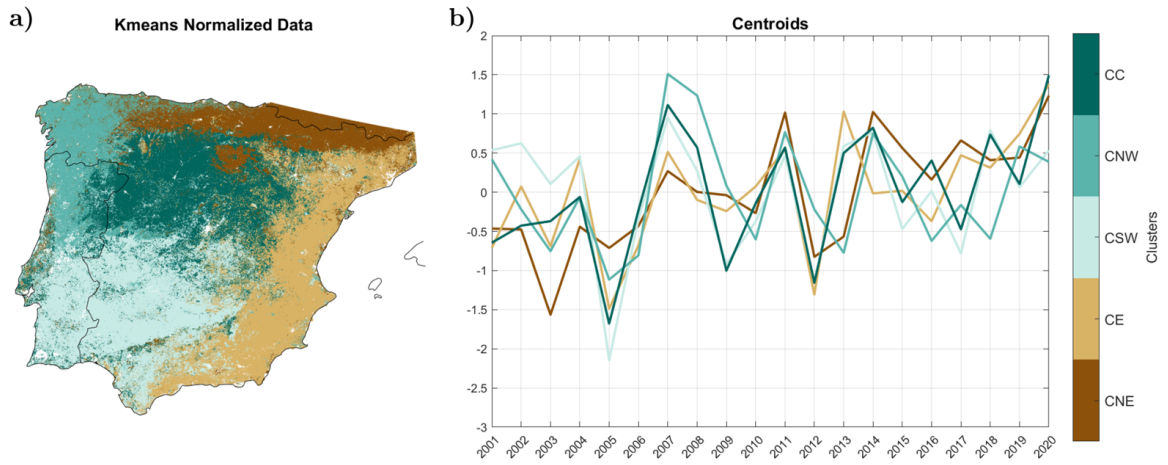

Figure 3.5: a) Spatial representation of the 5 clusters, where cluster CNE accounts for 14% of the total Iberian Peninsula area, cluster CE represents 23%, cluster CSW 27%, cluster CNW 12% and cluster CC 24%. b) Temporal representation of the normalized value of each cluster centroid.

Figure 3.5b) shows the evolution of the centroids of each cluster in the period 2001-2020. The signals of the main droughts that occurred in the period are clear. Firstly, the effects of the 2004-2005 drought are very present in all five clusters, although these effects are more visible in the clusters that have lower production (clusters CE, CSW and CC). Moreover, this drought had a massive impact on Southern and Central Iberia. For this reason, clusters CSW and CC, that are mainly situated in Central and Southern parts of the Iberian Peninsula, had major drops in production. Additionally, these two clusters and cluster CE are the three less productive clusters, as seen in Figure 3.6a), and are more susceptible to the impacts of extreme events. The 2009 drought impacted mainly clusters CSW and CC as the centre of the Iberian Peninsula was the region most affected by it (Liberato et al., 2021). The 2012 Drought was very widespread across all of the Iberian Peninsula (Liberato et al., 2021) and had very notable impact on all of the clusters, being that the least affected cluster was also the cluster with the highest production values among all of them. The drought of 2016-2017, one of the worst droughts in Europe in the last decades (Ayarzagüena et al., 2018), impacted mainly the southwestern part of the Iberian Peninsula, as it can be seen in clusters CSW, CNW and CC.

Figure 3.6a) shows the time series of the area averaged NPP in each of the 5 clusters. Albeit the cluster analysis be based in normalized data, it is clear that it separates regions with very different productivity. In fact, the averaged NPP in clusters CNE and CNW is about twice the averaged NPP in the other clusters. clusters CNE and CNW values range from 0.71 and 0.78 to 0.86 and 0.94 kg C/m^2, respectively, while the other three clusters values vary between 0.39 to 0.57 kg C/m^2.

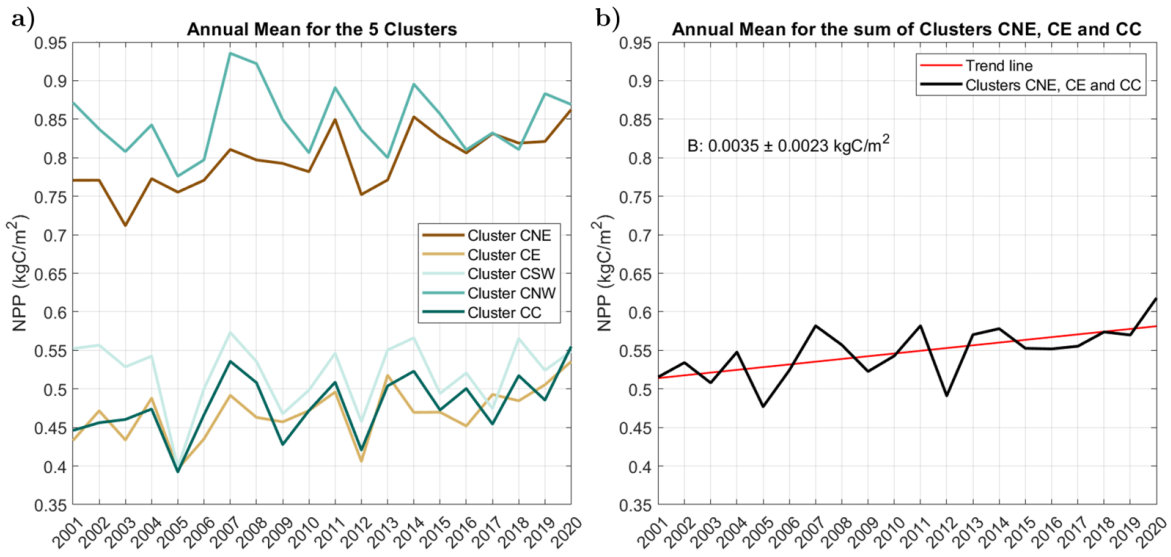

Figure 3.6: Time series of the area averaged NPP for: a) each of the 5 clusters. b) the sum of clusters CNE, CE and CC (black line), trend line (red) and the b values as well as its 95% confidence intervals

As was described before, clusters CE, CSW and CC present the lowest amounts of vegetation. In Figure 3.6a), the impacts of droughts in these clusters are very noticeable, especially during the 2005 and 2012 droughts, where the NPP values show a significant decrease from the year before. Moreover, in the year after these drops in NPP values, there is a recuperation with the NPP going to the values experienced in the year after the droughts. Furthermore, cluster CNE also presents this type of behaviour for 2012, as the drought is obvious. This contrasts with clusters CNE and CNW in 2003 and with cluster CNW in 2012. As in these cases, a significant reduction of NPP is not noticeable. This may be due to the climatic conditions as well as the types of vegetation cover present in each cluster.

A close inspection of Figures 3.5b) and 3.6a) suggests that the NPP, in the three geographically contiguous clusters CNE, CE and CC, presents a positive trend in the last twenty years. Additionally, from Figure 3.3, the areas covered with these clusters have the highest percentage points showing positive trends. For these reasons, these clusters have been grouped up and their joint evolution was studied in Figure 3.6b). In fact, the area averaged NPP, in the three clusters presents a statistically significant positive trend. In other words, there is an increase in the production in the three clusters for the 20 years. The trend is 0.035 ± 0.023 kg C/(m^2 $\cdot$ decade) at a p-level of 5%.

An analysis of land cover in each cluster (Figure 3.7) reveals that the clusters CNE and CNW are composed predominantly by Savannas (from here onwards Savannas written in full will refer both WSV and SV land covers) and ENF. The clusters CE,

CSW and CC are dominated by CP, GS, and Savannas land covers.

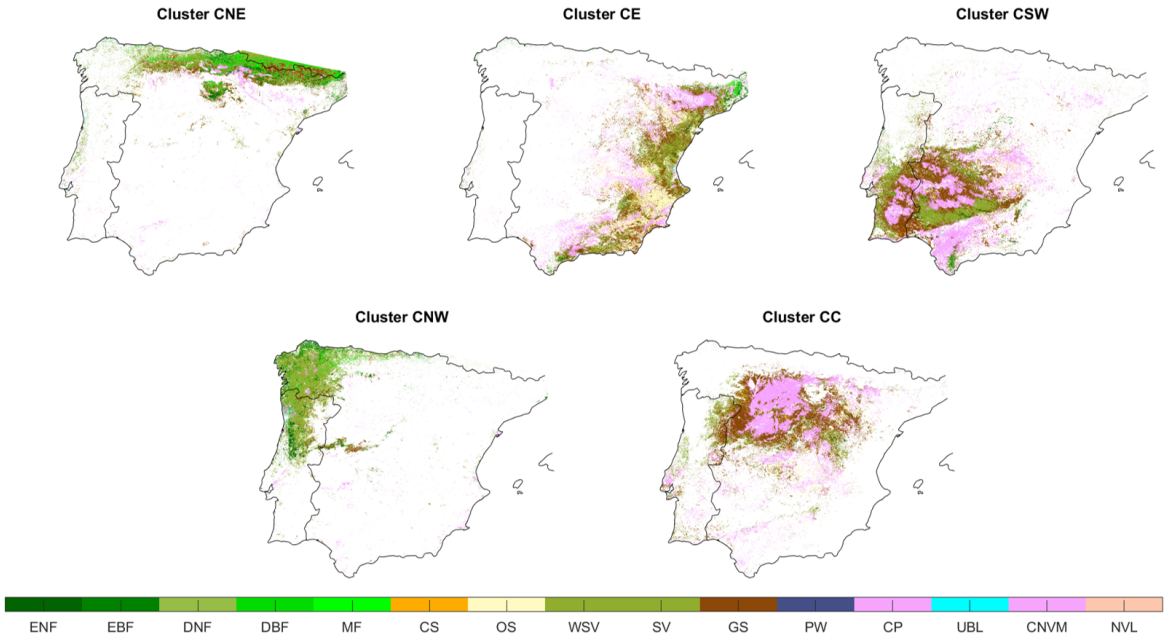

Figure 3.7: Land Cover distribution for each considered cluster.

To better understand the cause of the positive trend of the NPP, Figure 3.8 characterizes the productivity of each type of land cover, and Figure 3.9 shows the time evolution of the area of each land cover in the clusters CNE, CE and CC. Figure 3.9 was calculated by identifying the number of pixels of each land cover type for each year, after this the percentages of the total area that each land cover occupied was calculated. The large dispersion of NPP in the box plots of some land cover types in Figure 3.8 may be due to pixels with uncertain classification, i.e. from year to year some pixels have their land cover type changed. Due to this, some of this pixels prior to the change may have higher or lower NPP values than the mean values of its current classification, thus inducing large dispersion in the NPP values for the land cover.

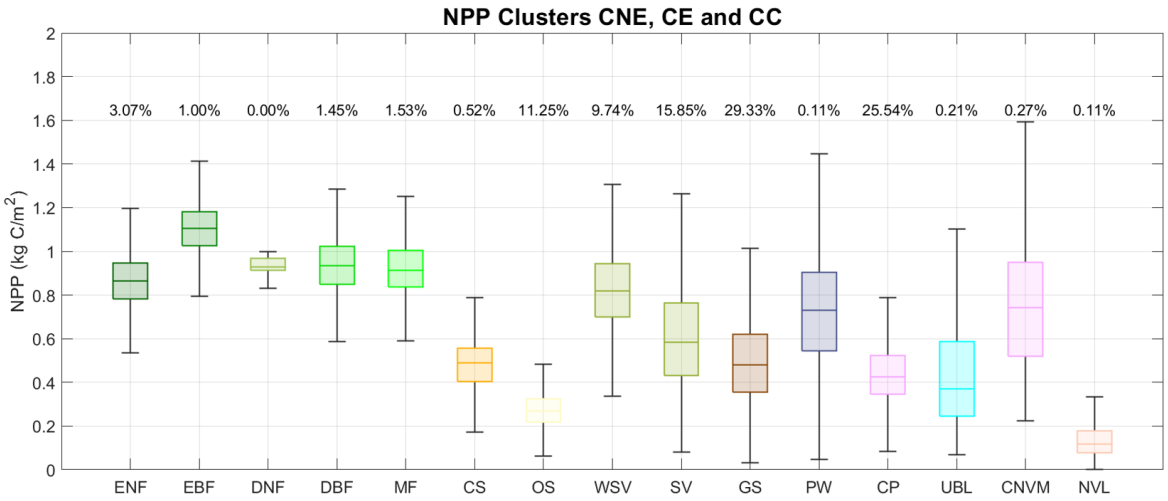

Figure 3.8: Box chart of each Land Cover type, where 50% of each land cover type is encompassed within the box, the outliers were not represented in this figure to retain visual clarity.

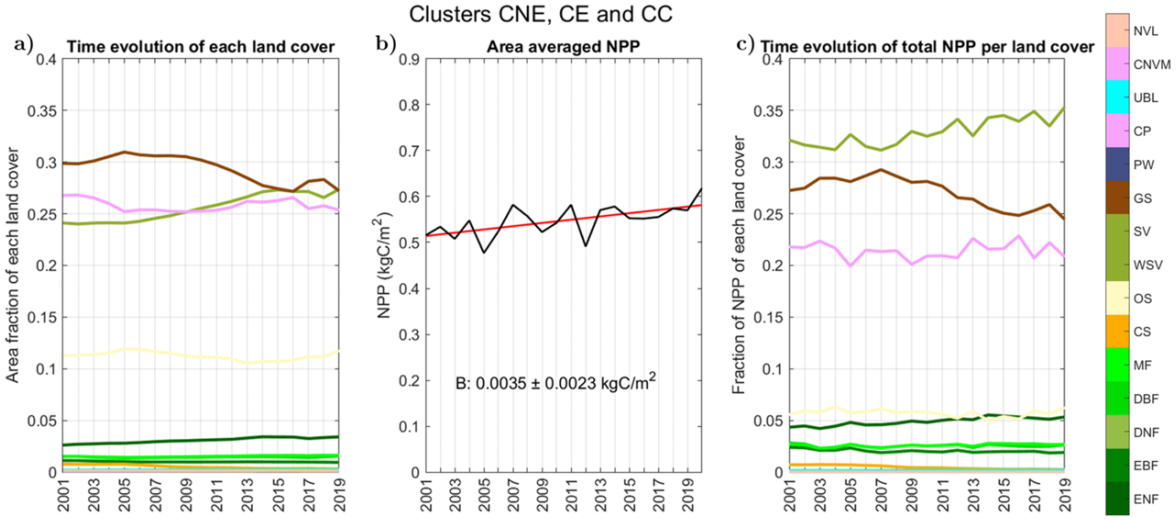

Figure 3.9: Land coverage time series analysis for clusters CNE, CE and CC. a) Percentage of pixels (area fraction) occupied by each land cover per year. b) Area averaged NPP (black) and associated trend (red). c) Percentage of NPP represented by each land cover per year. In a) and c) the colors of the curves for each land cover are the same as used in Figure 3.8.

The positive trend present in Figure 3.6 may be associated with the observed feature in Figures 3.8 and 3.9. The Savannas type has increased by 14% having gained roughly 17646 km^2[†], additionally, the Evergreen Needleleaf Forests (ENF) increased by 4285 km^2 which represents a 30% increase in the area dominated by ENF. The increases in these land cover types may be related to the reduction in 9% of the area of Grasslands

[†]The area is calculated counting the number of pixels. The area of each pixel is 0.250 km^2.

(GS), which corresponds to an absolute decrease of 14298 km^2 in the GS area. The area of Croplands (CP) presents great variability in the past 20 years but only looking at the values in 2001 and 2019 it is possible to see that this land cover type has lost 7594.5 km^2, which amounts to a 5% decrease. Furthermore, the area of Evergreen Needleleaf Forests (EBF) has decreased by 15%, losing a total of 962 km^2. Moreover, in the two Shrubland classes, there was a fluctuation in the area each represented, being that Closed Shrublands (CS) lost 60% of its area (-2499 km^2), while Open Shrublands (OS) gained 4% of its area (2451 km^2). In summary, the area lost by GS was probably replaced by Savannas and ENF, being that both have higher median NPP ($\approx$0.7 and $\approx$0.8, respectively) than the original vegetation cover ($\approx$0.5), as observed in Figures 3.8 and 3.9. So, the changes in the area of the different types of land cover may help to explain the positive trend observed for clusters CNE, CE and CC.

3.2 Land cover and NPP evolution in Portugal's mainland

The analysis of the trend of NPP averaged over clusters CNE, CE and CC suggests that it may be related to land cover changes (see Figure 3.9). In the last 20 years, substantial changes in land cover have been reported in Portugal's mainland, mainly associated with wildfires and/or changes in intensive monocultures in the Alentejo (Allen et al., 2018; Silveira et al., 2018).

In order to identify some of these land cover changes and try to understand their impact in the NPP, the yearly area fraction of each land cover and the yearly fraction of NPP per land cover were calculated for Portugal's mainland (Figure 3.10) and additionally for five subdomains, which include the large burnt area in 2017 (Figure 3.11) and the Portugal's regions of North, Centre, Alentejo and Algarve (Figure 3.12).

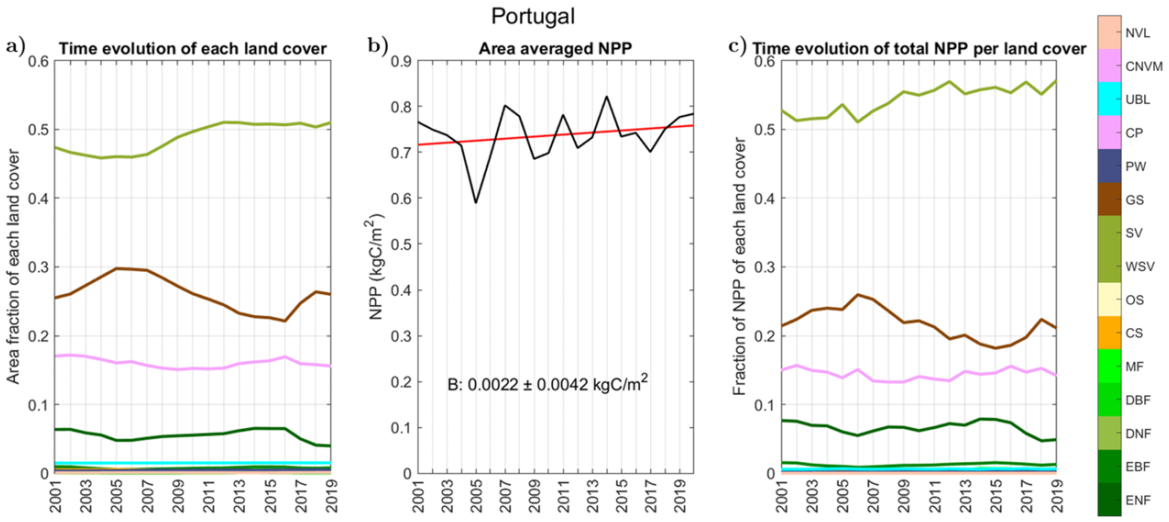

Figure 3.10: Land coverage time series analysis for Portugal. a) Percentage of pixels (area fraction) occupied by each land cover per year. b) Area averaged NPP (black) and associated trend (red). c) Percentage of NPP represented by each land cover per year. In a) and c) the colors of the curves for each land cover are the same as used in Figure 3.8 and 3.9.

Figure 3.10 shows a big reduction in areas classified as Grasslands (GS) from 2006 to 2016, more specifically, from 2006 to 2016 the area of GS was reduced by about 10060 km^2 (25%). The GS may have been replaced by Savannas and Evergreen Needleleaf Forests (ENF) since the areas of these land cover types grew by 9% (5648 km^2) and 28% (1965 km^2), respectively. In contrast, from 2016 to 2019 there was a decrease in ENF and Croplands (CP) of 38% (3390 km^2) and 8% (1782 km^2), respectively, and an increase in GS of 18% (5266 km^2). This pattern is very characteristic of post-fire vegetation evolution, as GS are composed of "herbaceous annuals" which are a group of plants that only present vegetative activity during their sole growing season and are known to quickly populate areas affected by fires (Keeley et al., 1981). Moreover, the decrease in ENF quantities goes in accordance with the 2017 wildfires that affected vast areas populated with this land cover type (ICNF, 2017). In fact, performing a similar analysis to that of Figure 3.10 but restricted to the burnt areas of 2017, the impact on the changes of land cover is clear (Figure 3.11). In the 2017 burnt area a whopping 97% of ENF classified pixels changed classification in the three years after the fire, this amounts to 7696 pixels (1924 km^2). This is nearly 60% of the total ENF area lost in Portugal during the period 2016-2019. This land cover shifted to Savannas and GS as observed in Table 3.2. Table 3.2 presents the evolution of the ENF classified pixels over the 2017 burnt areas for the year before (2016, the control year) and after (2018, 2019) the 2017 fire event. The 2017 values must be read with caution because the land cover types are produced yearly and, for that reason, these values includes a mix of pre- and

post-fire vegetation data.

The Figures 3.10b) and 3.11b) do not show any statistically significant trend in the NPP. The impacts of wildfires and droughts in NPP are clear in Figure 3.11b). In fact, the 2017 burnt area shows a strong negative anomaly in the NPP in 2018. The effect of the drought of 2004-2005 is also evident in the strong negative anomaly seen both in figures 3.10b) and 3.11b). Moreover, as we will refer later, some burnt areas of the 2003 wildfires coincide with part of the burnt area of the wildfires in 2017.

Table 3.2: Evolution of the land cover type of the ENF classified pixels in the control year (2016) that burnt in the October 2017 wildfires. The 2017 values must be read with caution because the land cover types are produced yearly and, for that reason, these values includes a mix of pre- and post-fire vegetation data.

	2016	2017*	2018	2019
ENF	7696	4384	690	0
EBF	0	1	1	4
DNF	0	0	0	0
DBF	0	0	0	0
MF	0	15	0	0
CS	0	0	5	4
OS	0	0	0	0
WSV	0	3065	4906	6036
SV	0	202	538	771
GS	0	22	1412	858
PW	0	7	144	23
CP	0	0	0	0
UBL	0	0	0	0
CNVM	0	0	0	0
NVL	0	0	0	0

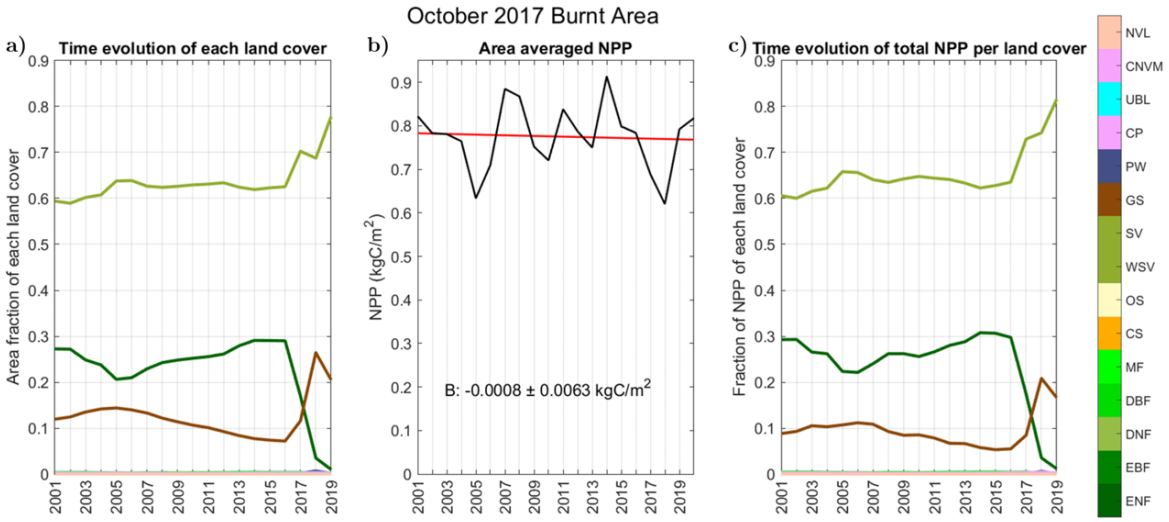

Figure 3.11: Land coverage time series analysis for Portugal's 2017 burnt area. a) Percentage of pixels (area fraction) occupied by each land cover per year. b) Area averaged NPP (black) and associated trend (red). c) Percentage of NPP represented by each land cover per year. In a) and c) the colors of the curves are the same as the respective curves in Figure 3.9 and 3.10.

We repeated the analysis over Alentejo, Algarve, the North and Centre regions of Portugal to see if any signal can be observed in the land cover and NPP data.

In Figure 3.12 we can see that all four regions have the same qualitative behaviour although from region to region the values differ. Observing Figures 3.11 and 3.10 alone, they seem to suggest that the land cover changes after 2016 may be associated with the large wildfires of 2017. However, a similar change pattern (decrease in ENF and increase in GS) is observed across all the regions (Figure 3.12), even for those where wildfires are not expected to have had a high impact. Therefore, there must be other factors influencing this variability identified in the 2017-2019 period. To identify such factors a more in depth study using a more appropriate Land Cover dataset with better resolution would be employed. In fact, as written in the user guide of the NPP product (Running and Zhao, 2019), "given its global nature..., a broad classification scheme, which retains the essence of land cover, is necessary. Since Collection 6 MODIS products are designed at a 0.5-km grid scale, it can be difficult to obtain accurate land cover in areas with complex vegetation, and misclassification can occur. However, studies have suggested that the MODIS vegetation maps are accurate to within 65-80%, with higher accuracies for pixels that are largely homogeneous, and allow for consistent monitoring of the global land cover."

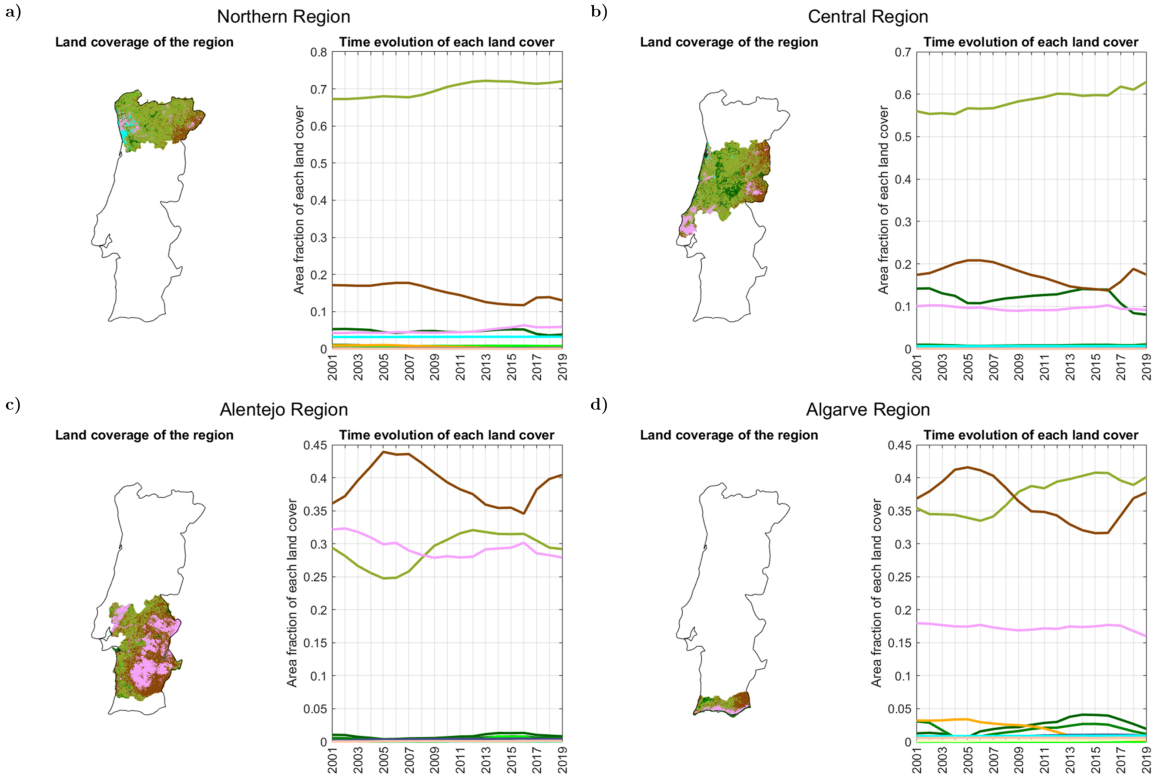

Figure 3.12: Land cover representation for each considered area and time series of the percentage of total pixels (area fraction) occupied by each land cover per year. a) North Region b) Centre Region c) Alentejo and d) Algarve.

Albeit the land cover scheme used in the NPP and GPP products does not seem to have enough detail to characterize land use changes occurred in south of Portugal, it captures a clear and consistent signal in the changes in land cover due to large fires (see left panel in Figure 3.11).

The impact in the NPP of the burnt area is also noted in the middle panel of Figure 3.11, in particular for the wildfires in the years of 2003, 2005 and 2017 (parts of the burnt areas in 2003 and 2005 burnt again in 2017). Figure 3.13 and 3.14 give more details for the burnt areas in four of the years that had major wildfires in mainland Portugal.

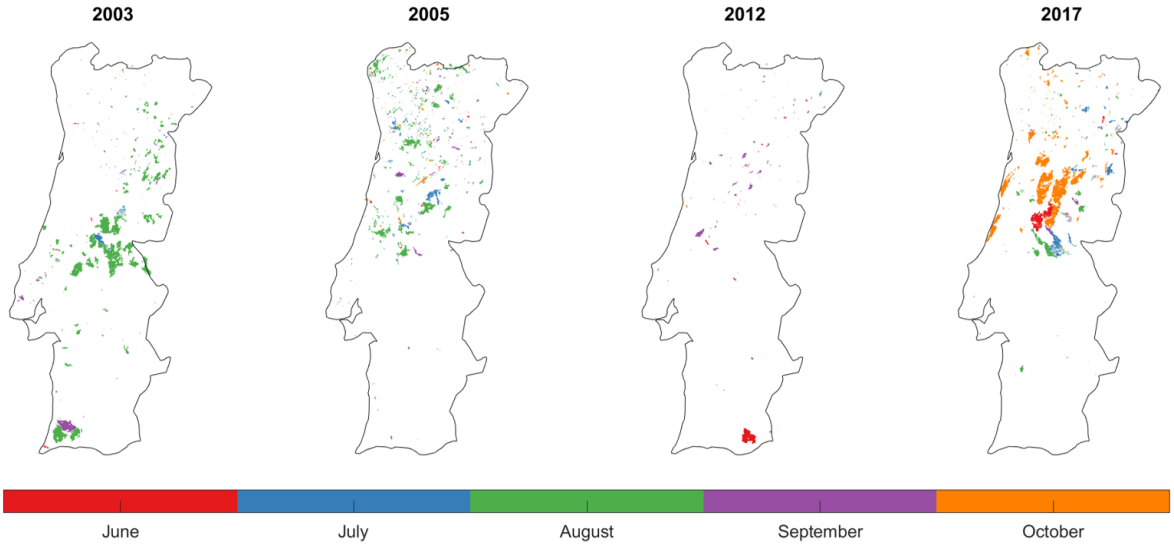

Figure 3.13: Burnt area maps for 2003, 2005, 2012 and 2017 in the Portugal. Red pixels depict wildfires that started in June, blue pixels burnt in July, green pixels burnt in August, purple pixels burnt in September and orange pixels burnt in October

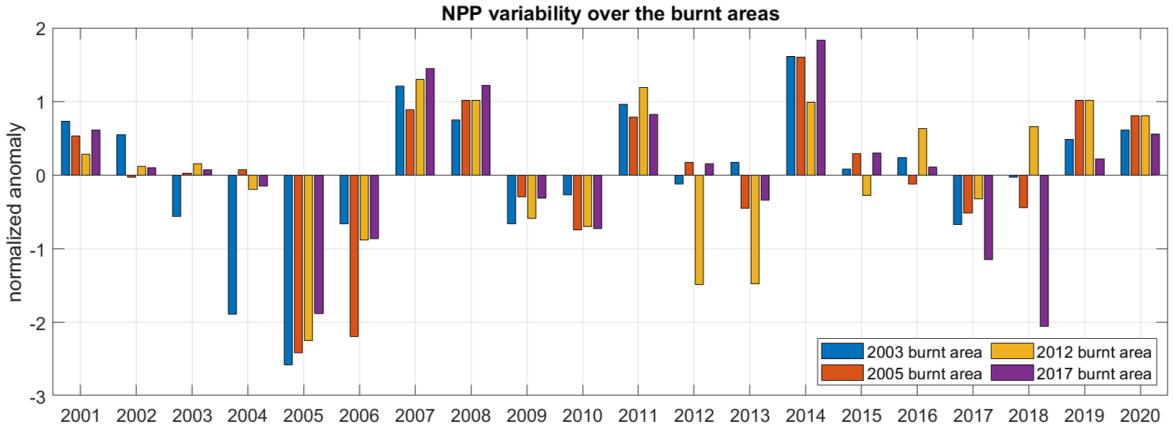

Figure 3.14: Anomalies of the area averaged NPP in the burnt areas of the wildfires of 2003, 2005, 2012 and 2017.

In Figure 3.13, the burnt areas for the wildfires that occurred in 2003, 2005, 2012 and 2017 are depicted by the month they occurred in. To see the loss of NPP in the burnt areas and the recovery of its annual values, we calculated the anomalies of the area averaged NPP in the 20-year period from 2001 to 2020. Considering separately the burnt area in each of the four years, we calculated the area averaged annual NPP for the whole 20-year period. Then, the time mean and the anomalies of the obtained time series were calculated. Finally, the anomalies were normalized by the STD of the respective time series. Figure 3.14 shows the anomalies of the four time series.

Figure 3.14 shows a decrease of NPP values in the years of high fire activity. In the years after the fire, NPP also presents strong negative anomalies, which is to be expected as the vegetation takes time to fully develop. Additionally, the recovery is impacted heavily by droughts that impose harsh climatic conditions on the young vegetation which affect their growth capabilities.

For the 2003 burnt area, the NPP continues to drop until it reaches its lowest value in 2005, as it can be seen in Figure 3.14. This is probably due to the drought that hit the Iberian Peninsula in 2004-2005. The vegetation in this area only shows a slight recovery in 2006. Moreover, in the other three areas considered there is a steep drop in NPP values in 2005. This remarkable decrease may be associated with the impact the 2004-2005 drought had, not only in vegetation recovery post-fire but in vegetation as a whole.

In 2005 the wildfires still occurred during a drought year, due to this the vegetation presented little signs of recuperation in the following year. Two years after, in 2007, this area had very high NPP levels, meaning that a significant recuperation of vegetation productivity happened.

Likewise, the 2012 wildfires occurred during an active drought event, the impacts of the extreme conditions are very notable as in the next year the vegetation showed barely any signs of recovery. A considerable recovery occurred during 2014, but this burnt area showed little signs of recovery in the following years, one of the reasons that probably impacted this recovery was the 2016-2017 drought that affected the recovery of the vegetation in this area.

Finally, in 2017 the burnt area had its minimum NPP value the year after, one of the reasons is that part of these wildfires occurred in the last quarter of the year, as NPP is a yearly accumulation the burnt area registered normal NPP values during two-thirds of the year. For that reason, the large impact of these wildfires is only shown in the 2018 anomalies. The other reason is that these wildfires occurred simultaneously with a drought that extended from 2016 to the first months of 2018. As is normal, this impacted the vegetation's capabilities to regrow after the fire. This area showed a great increase in NPP values in the year 2019. The values registered for NPP in 2019 are very similar to the ones in the year before the fire in 2016.

In order to assess how many pixels of each land cover type burnt during each fire season, the burnt area data was compared to the Land Cover dataset. For this, the percentage of burnt area as a function of the land cover type was calculated and the results are shown in Table 3.3.

Table 3.3: Percentage of burnt area in Portugal as a function of the land cover type obtained for the year that preceded the 2003, 2005, 2012 and 2017 wildfires.

	ENF	EBF	DNF	DBF	MF	CS	OS	WSV	SV	GS	PW	CP	UBL	CNVM	NVL
2003	10.91	3.78	0	0.01	0.05	0.30	0.03	19.41	32.97	29.40	0.07	3.02	0.02	0.03	0.00
2005	18.21	1.28	0	0	0.40	0.13	0	39.15	27.71	12.10	0.09	0.58	0.20	0.15	0
2012	8.06	0.03	0	0	0.16	0.60	0.03	24.45	23.78	41.29	0.10	1.24	0.03	0.23	0
2017	29.01	0.26	0	0	0.40	0.12	0	44.14	18.39	7.19	0.14	0.19	0.05	0.11	0

The burnt area of 2003 consisted in 29% of Grasslands (GS), 33% of savannas (SV), 19% of Woody savannas (WSV) and 11% of Evergreen Needleleaf Forests (ENF). The two major land cover types burnt in this fire represent 62% of the total area, this explains the low mean value of NPP for this area since GS as a median NPP of roughly 0.5 kg C/m^2 and Savannas have a median value of approximately 0.65 kg C/m^2.

In 2005 most of the burnt area was WSV (39%), followed by SV (27%) and ENF (18%). As 39% of the burnt area is composed by WSV which has median NPP values of 0.82 kg C/m^2, this makes this burnt area have high overall NPP values. Additionally, the 18% of ENF also highly impact the overall NPP values, as this land cover type presents median NPP values of about 0.87 kg C/m^2.

The principal land cover type present in the burnt area of 2012 was GS, with 41%. As it was mentioned before, GS has a mean NPP of 0.5 kg C/m^2. Therefore, this area presents low NPP values, ranging from 0.59 to 0.78 kg C/m^2. Also, this burnt area had the lowest percentage of Forests of the four considered fire seasons. In addition, it should be noted that the 2012 wildfires presented the smaller amount of pixels burnt.

In 2017, 44% of the burnt area was composed of WSV and 29% was composed of ENF. The amount of ENF burnt in these wildfires was very significant when compared to the other years, specially since this burnt area had the highest amount of pixels burnt. Due to this, many of the wildfires registered in this year may have been classified as forest fires. This is worth mentioning because the vast majority of fires in Portugal are classified as rural. Additionally, this high percentage of ENF burnt is due in part to the October 15th wildfires that affected Leiria's National Pinus Forest.

3.3 Post-fire vegetation recovery

The NPP represents the net yearly integrated productivity and, due to the annual temporal resolution, does not have the adequate temporal resolution for a detailed analysis of the post-fire vegetation dynamics. A high time resolution can be provided by the GPP data. In fact, the GPP are available at 8-day intervals. At this time resolution, the data proved to be very noising for our analysis purposes and were smoothed using a moving average. Several values for the window of the moving average were tested and the chosen value was seven. This means that the value of a given point is influenced by

the value of the three points before and the three points after. This window represented a good balance between a cleaner signal while retaining the characteristics of the original data with a time resolution deemed to be adequate for the study of post-fire vegetation recovery. In this study, the following vegetation recovery model, initially proposed by Gouveia et al. (2010), was applied to the 2003 and 2017 burnt areas.

3.3.1 Vegetation Recovery Model

Gouveia et al. (2010) developed a monoparametric model for vegetation recovery using developed the NDVI vegetation index. Here we made an adaptation of the model to be applied to GPP data, which represent the carbon rate trapped by vegetation. In its original version, the model used an asymptotic annual cycle to represent a healthy equilibrium state of vegetation throughout the phenological year. Such ideal phenological cycle should be represented by a periodic $NDVI^*(t)$ function, with a period of one year. Defining the lack of greenness, y, as

$$y(t) = NDVI(t) - NDVI^*(t) \tag{3.1}$$

where $NDVI(t)$ is the actual value of the NDVI observed at time t, the instantaneous rate (dy/dt) of vegetation recovery was assumed to be proportional to the lack of greenness

$$\frac{dy}{dt} = -\frac{y}{\tau} \tag{3.2}$$

where τ is the time scale for the vegetation recovery. The minus sign ensures that the recovery rate is positive since the time scale of recovery is always positive. Equation 3.2 is the condition for an exponential relaxation to the equilibrium state, and its solution is

$$y(t) = ae^{-\frac{t}{\tau}} \tag{3.3}$$

where a represents the lack of greenness after the fire event, which is assumed to have occurred at the initial time t=0.

$$a = NDVI(t = 0) - NDVI^*(t = 0) \tag{3.4}$$

The value a can be taken as an indicator of fire damage as it is the largest value of the lack of greenness time series.

In practice, the ideal $NDVI^*$ annual cycle is determined by finding the maximum values of the NDVI for each calendar time, i.e., each week or month of the year. For example, considering monthly time series, the $NDVI^*$ for January is maximum NDVI

value from the values for all January months in the time series. The obtained annual cycle is referred as the Gorgeous Year (GY) as in Gouveia et al. (2010).

To apply a similar model based in the GPP data, we need to redefine $y(t)$ as the lack of carbon uptake by the vegetation. Because the annual cycle of the GPP has a large amplitude (see Figure 3.15), the lack of carbon uptake, $y(t)$, must be analysed in terms its fractional values instead of absolute values.

$$y(t) = \left(\frac{GPP(t) - GPP^*(t)}{GPP^*(t)} \right) = \left(\frac{GPP(t)}{GPP^*(t)} - 1 \right) \tag{3.5}$$

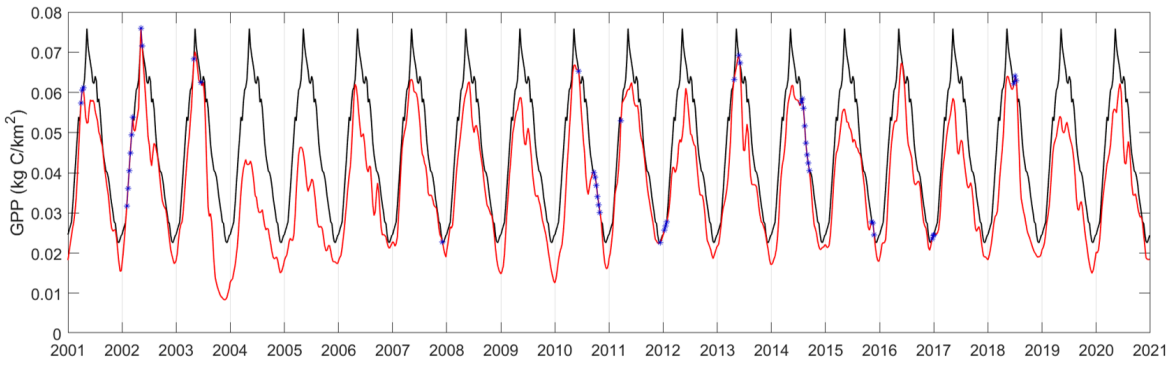

Figure 3.15: Time series of the Gorgeous Years, represented with a black line, and the GPP values (red) for a given area.

Figure 3.16 shows the normalized anomaly, i.e., the fractional lack of carbon uptake flux (red line) and the absolute values (blue line) for the GPP averaged over the burnt areas in 2003. A clear seasonal cycle can be observed in the absolute lack of carbon uptake in a number of years after 2003. Such seasonal cycle is less observable in the fractional lack of carbon uptake.

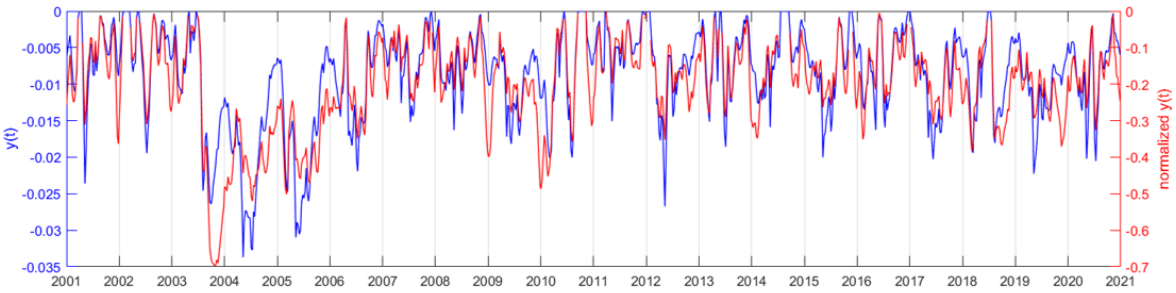

Figure 3.16: Time series of the anomaly (blue) vs normalized anomaly (red) values.

If we replace a by y(0) and $1/\tau$ by b in Equation 3.3 the following linear model in b is obtained.

$$\ln\left[\frac{y(t)}{y(0)}\right] = -bt \tag{3.6}$$

The parameter b can be estimated by means of a linear regression. We also tested the calculation of the parameter b by using method of least square deviation in Equation 3.3 and the values of b are not significantly different from the obtained by the linear regression. The recovery time scales presented in this work were obtained by linear regression as in Gouveia et al. (2010, 2018) and Bastos et al. (2011).

3.3.2 Sensitivity of the estimated recovery time to the length of the time series.

After a fire event, the vegetation will evolve in direction to its ideal equilibrium state, represented by the GY cycle. However, before or after the vegetation have completely recovered, it may be affected by a successive fire event or by strong droughts, which will bring new lack of carbon uptake unrelated with the initial event. It is, therefore, important to use a time series window large enough to a correct estimation of the recovery time, but as short as possible to avoid contamination by other events.

Another important issue for the curve fitting is related with the empirical determination of the ideal GY cycle. Because the dependent variable is $\ln\left(y(t)/y(0)\right)$, where $y\left(t\right) = \left(GPP\left(t\right) - GPP^{*}(t)\right)/GPP^{*}(t)$, it may take infinite negative values if some values in the window of fitting are used to define the GPP^{*}. The points, in the window of fitting, with $y\left(t\right) = 0$, were not used in the regression estimation of the recovery time.

Figure 3.17 shows the time series of lack of carbon uptake based on the GPP averaged in the area burnt by the wildfire in Monchique at the year of 2003. The dashed horizontal line indicates a fractional lack of carbon uptake of 10%. Following a criterion similar to that used by Gouveia et al. (2010) and Bastos et al. (2011), we assume that the vegetation recovered from the fire when $y(t) > -0.1$.

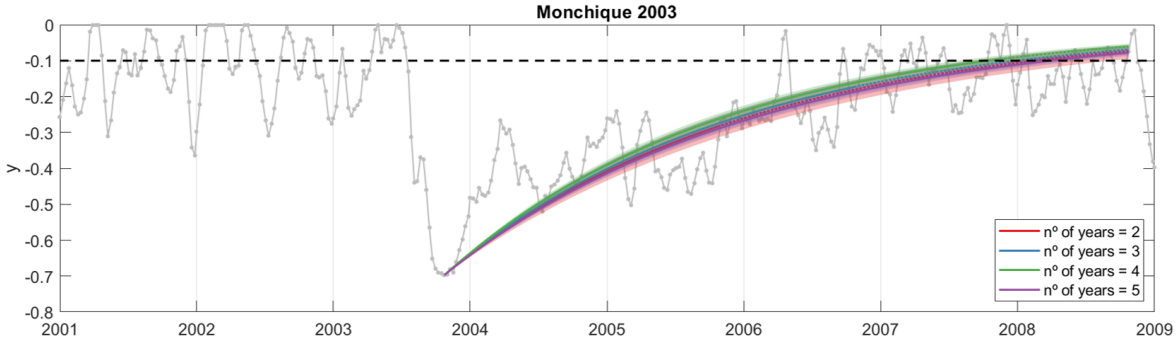

Figure 3.17: Time series of observed (lines with asterisks) and modelled (thick coloured curves) values of 8-day composite values of lack of carbon uptake, y, over the large scars of the fire in Monchique in 2003. The modelled curves were obtained for different fitting time windows after the fire, namely 2 (red), 3 (blue), 4 (green) and 5 (purple) years. Each curve was drawn as a solid line in the respective fitting time window and prolonged by a dotted line in order to all curves represent the same period of time. The shaded bands indicate the 95% confidence intervals. The horizontal dashed line represents the level of vegetation recovery defined as y(t)=-0.1.

Four regression curves, calculated considering windows of 2, 3, 4 and 5 years, are also shown in Figure 3.17 and the respective estimated times of recovery are given in Table 3.4. The values are relatively consistent with a dispersion smaller than 10%. The choice of a window of 4 years seem to be adequate, because the reference line of y= -0.1 is approached by all curves and the data, and the strong anomalies at the end of 2008, certainly not related with the fire in 2003, can be avoided. Therefore, in the next cases to be analysed, a time window of 4 years will be used to perform the regression.

Table 3.4: Results of the recovery model for each length of the dataset considered.

	tR (months)	I95[tR]
2 years of data	53	[47,60]
3 years of data	51	[47,56]
4 years of data	49	[46,52]
5 years of data	54	[51,57]

3.3.3 Case Studies

Monchique 2003

In 2003, the region of Mochique in Algarve was affected by large fires. The burnt areas in that fires are shown in the left panel of Figure 3.18. The west and east areas (red and blue respectively) burnt during August, while the northernmost area (green) burnt in September. The three right panel show the time series of the GY cycle (black lines) and the area averaged GPP (coloured lines) for each one of the three burnt areas. The colour of each line is the same as the area in the left panel that they represent.

The NPP values that were used to define the GY cycle in each area are marked with cyan asterisks. In all three areas is possible to see that, around halfway through 2003 the GPP values for all areas dip and slowly crawl back up with time.

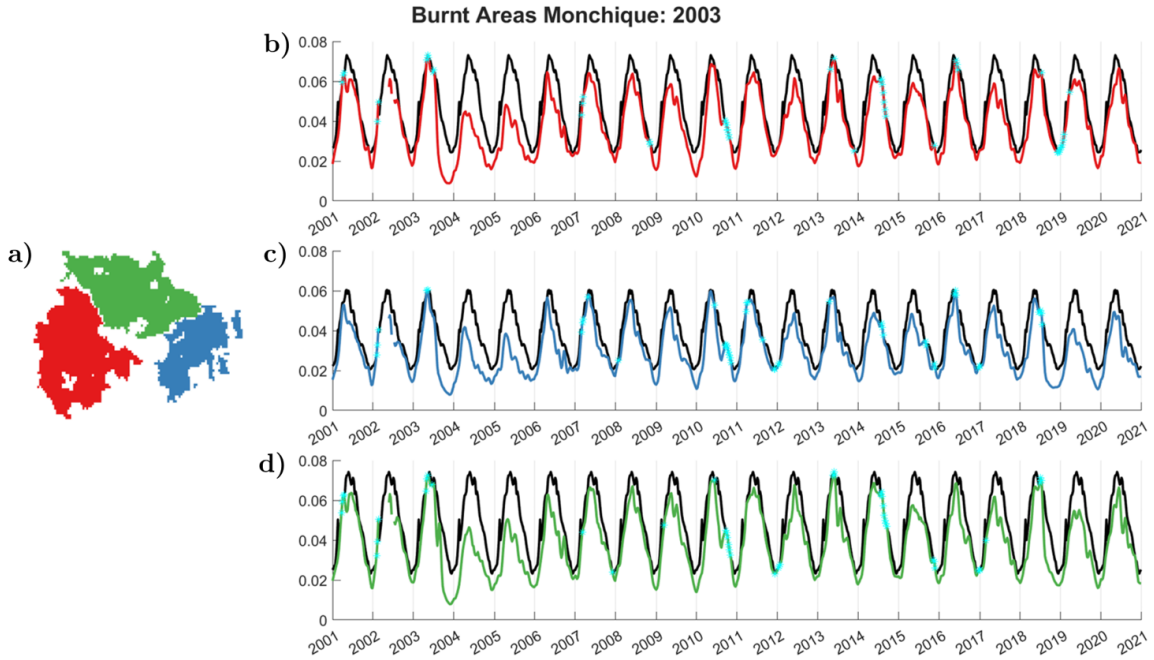

Figure 3.18: Monchique 2003 a) burnt area subdivision and annual GPP cycle vs GY for b) West c) East and d) North Monchique area.

The evolution of the land cover for the pixels that represent the burnt areas in Figure 3.18, since the year before the fire just to 4 years after, is shown in Figure 3.19. It is possible to see the impacts the 2003 fire had on the vegetation of the burnt area. From 2002 to 2003 is evident a reduction in the quantity of land covered by forests (ENF and EBF). As this product is produced once a year, it integrates the vegetation present year-round. So, the full change in vegetation cover can only be assessed in the following year, and, as expected, the year 2004 presents major changes as almost all the extent of land that was coded as ENF and EBF is now classified as Savannas, which is coded as transitional vegetation in other land cover classifications with higher spatial resolutions, such as Corine Land Cover (Gouveia et al., 2010). In 2007/2008 the vegetation appears to have recovered almost completely in terms of Forest (48 months). As the fire occurred in 2003, the 2002 land cover map represents the normal undisturbed vegetation cover of the area. The fraction of each vegetation type, in the year before the fire, is shown in Figure 3.20. The most prominent vegetation classes in the total area are ENF, EBF, SV, WSV and GS. However, as can be inferred from the right panel in Figure 3.20, the distribution of vegetation is unequal in the three subareas. The northernmost area is mainly dominated by EBF, ENF and Savannas, with very

few pixels classified as GS. The western area has a fifty-fifty distribution of Savannas and EBF, whilst many pixels represent GS. The eastern area is practically only covered by Savannas and GS.

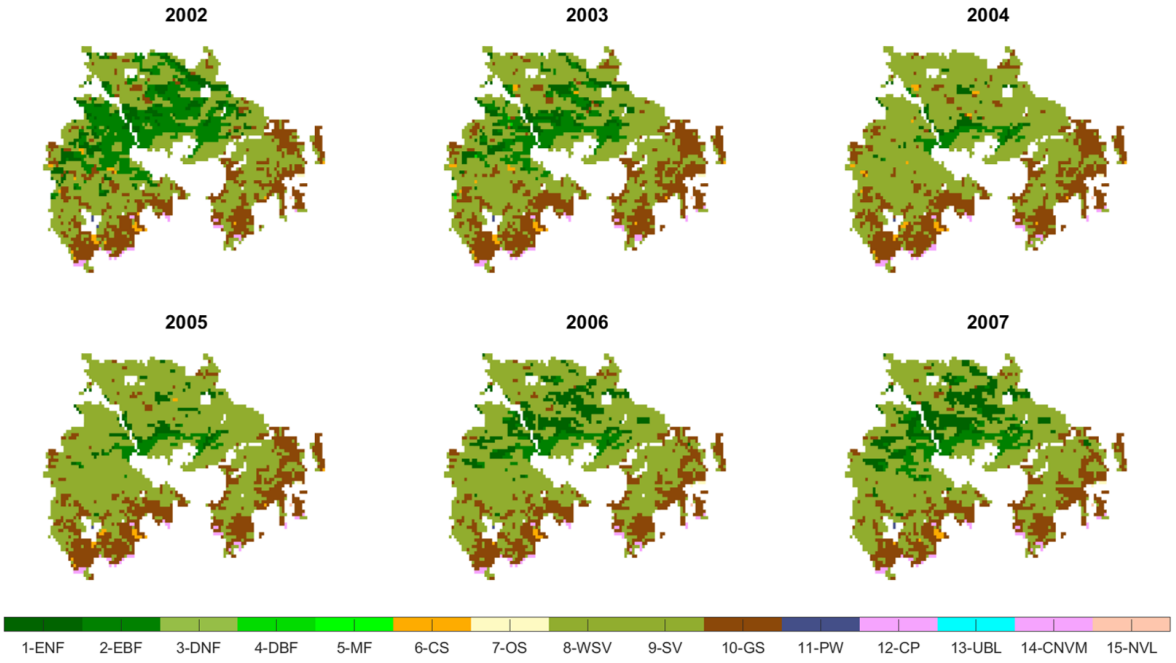

Figure 3.19: Evolution of the land cover for the pixels that represent the burnt areas in Figure 3.18, since the year before the fire just to 4 years after.

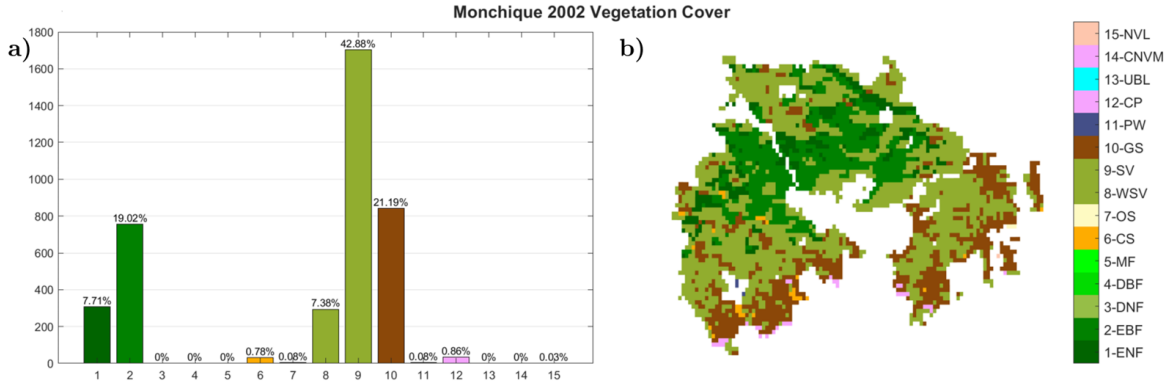

Figure 3.20: Monchique burnt area a) percentage of each land cover type and b) the land cover distribution for the year that preceded the fire.

The impact of the fires in the GPP can also be noticed in the maps of its seasonal means. Figure 3.21 shows the averaged GPP values for March, April, and May (MAM, Spring), July, August, and September (JAS) and October and November (ON), both for the burnt area and for a larger region including the burnt area. Results show that in Spring, where usually production values are higher, all these values are very homogeneous. This is not the case for JAS, where evidently the west and east areas

have lower values than the north-most area. Since the latter only burnt in September whilst the other two burnt in August.

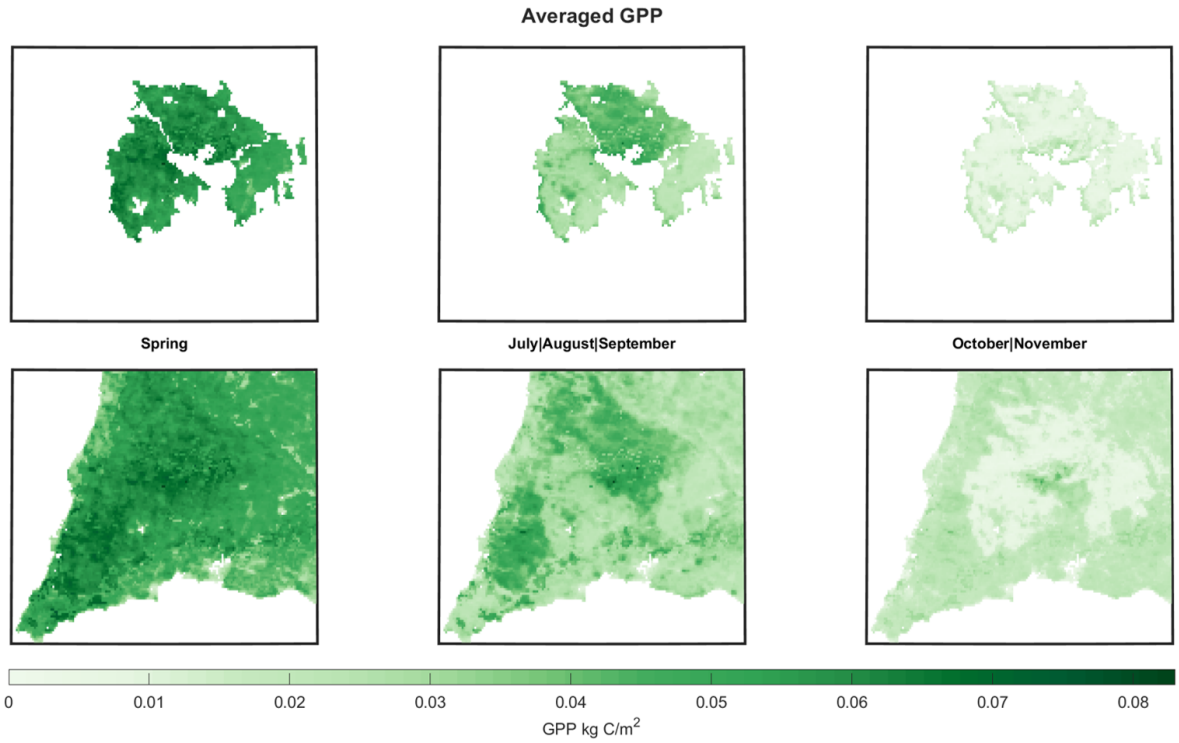

Figure 3.21: Monchique burnt area averaged GPP for Spring, July|August|September and October November.

A much detailed analysis of the time evolution of the vegetation recovery can be obtained by analysing the 8-day values of the GPP. In Figure 3.17, the vegetation recovery model was applied to the whole burnt area of Monchique in 2003. However, the wild fires in each one of the subareas of Figure 3.18 occurred in different dates and the vegetation differs between the subareas (see Figure 3.13 and 3.20). To see if the differences impact substantially the recovery time of the GPP, we applied the model to each subarea. The results are shown in Figure 3.22 and Table 3.5. All areas presented the same recovery time estimates of forty-seven months while the 95% confidence levels vary from three to four months of this value. The results are slightly unexpected as the vegetation cover of the three areas is different and, *a priori*, we could expect that different vegetation types would present different recovery times. The analysis of the recovery time in function of the vegetation type before the fires (Table 3.6 and Figure 3.23) also does not show a clear difference, except for GS which shows a faster recovery. The shorter recovery time for GS is as expected since this land cover type is dominated by herbaceous annual plants which grow rapidly during the growing season and die at the end of it to give way to new vegetation. So, the discrepancy from this land cover to the other three is easy to understand since, contrary to GS, these are dominated

by trees. The closer values of recovery for the other three types of vegetation can be understood as the recovery of the GPP capacity is not the same as the recovery of the land cover type present before the fire, and different land covers may have similar efficiency for the CO_2 uptake (see Figure 3.8).

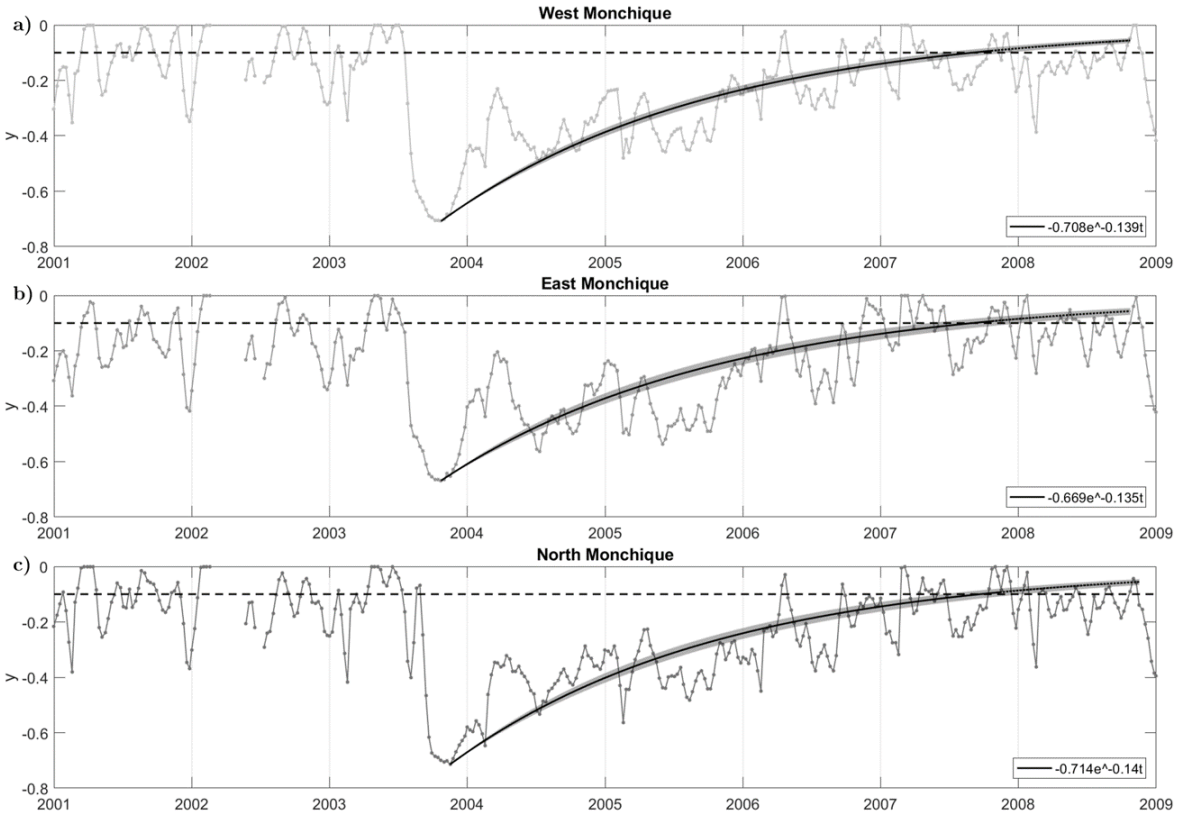

Figure 3.22: Time series of observed (lines with asterisks) and modelled (thick curves) values of 8-day composite values of lack of carbon uptake, y, over three subareas of the large scars of the 2003 Monchique fires: a) West, b) East and c) North Monchique subarea. The shaded bands indicate the 95% confidence intervals. The horizontal dashed line represents the level of vegetation recovery defined as y(t)=-0.1. (The analytical expression of the fitted curves are given in the lower right corner of each panel, with the unity time, t, equal to 100 days.)

Table 3.5: Recovery times and 95% confidence intervals for the three areas.

	tR	I95 [tR]
West Monchique	47	[44,50]
East Monchique	47	[43,52]
North Monchique	47	[44,51]

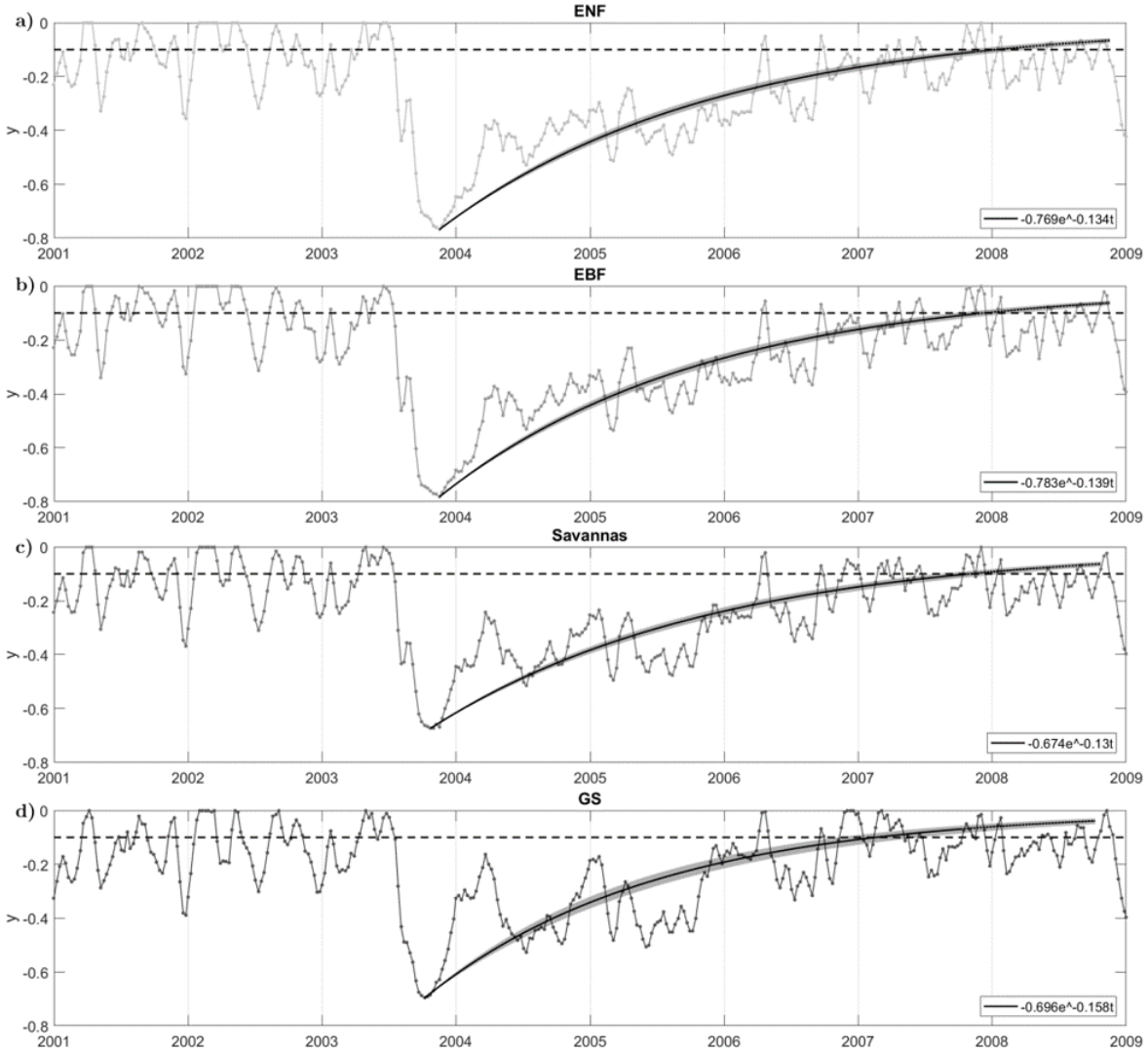

Figure 3.23: Time series of observed (lines with asterisks) and modelled (thick curves) values of 8-day composite values of lack of carbon uptake, y, over the most prominent land covers in the Monchique 2003 burnt scar: a) Evergreen Needleleaf Forests (ENF) b) Evergreen Broadleaf Forests (EBF) c) Savannas (SV and WSV) and d) Grasslands (GS). The shaded bands indicate the 95% confidence intervals. The horizontal dashed line represents the level of vegetation recovery defined as y(t)=-0.1. (The analytical expression of the fitted curves are given in the lower right corner of each panel, with the unity time, t, equal to 100 days.)

Table 3.6: Recovery times and 95% confidence intervals for the most prominent land cover types.

	tR	I95 [tR]
ENF	51	[48,54]
EBF	50	[47,52]
Savannas	49	[46,52]
GS	41	[38,45]

The results from Gouveia et al. original paper suggested recovery times of forty-three months for this area, with a 95% confidence interval from thirty-eight to forty-nine months. The values obtained here for the same area are within this confidence level, which validates the model adaptation presented here.

Wildfires in October 2017

The central region of Portugal was affected by large fires in October 2017, which occurred under drought conditions and strong wind due to the passage of the storm Ophelia off the cost of Portugal. These wildfires were ones of the more devastating in recent memory. These left big burnt scars and had a major impact on the vegetation. Figure 3.24 represents the land cover evolution of the 2017 burnt area.

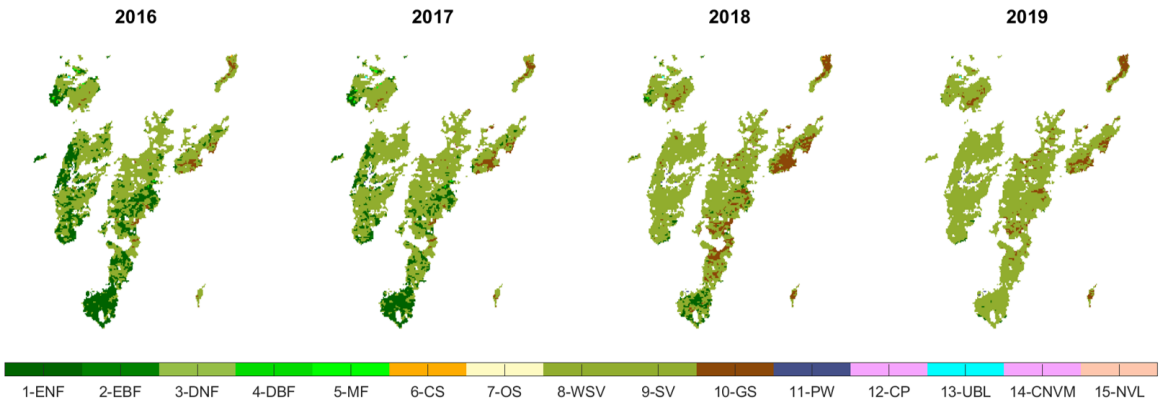

Figure 3.24: Central Region burnt area land cover evolution 2016-2019.

The annual cumulative GPP was calculated and presented in Figure 3.25. In the same way, as for the other region, in the year after the fire, the decrease in GPP is very clear. Moreover, this discrepancy in values is even more evident due to the fact that this fire occurred in October, and for that reason, almost ten months of that year presented normal production values. Furthermore, from the analysis of these graphs is possible to assume that the GPP capacity has most likely fully recovered in 2021.

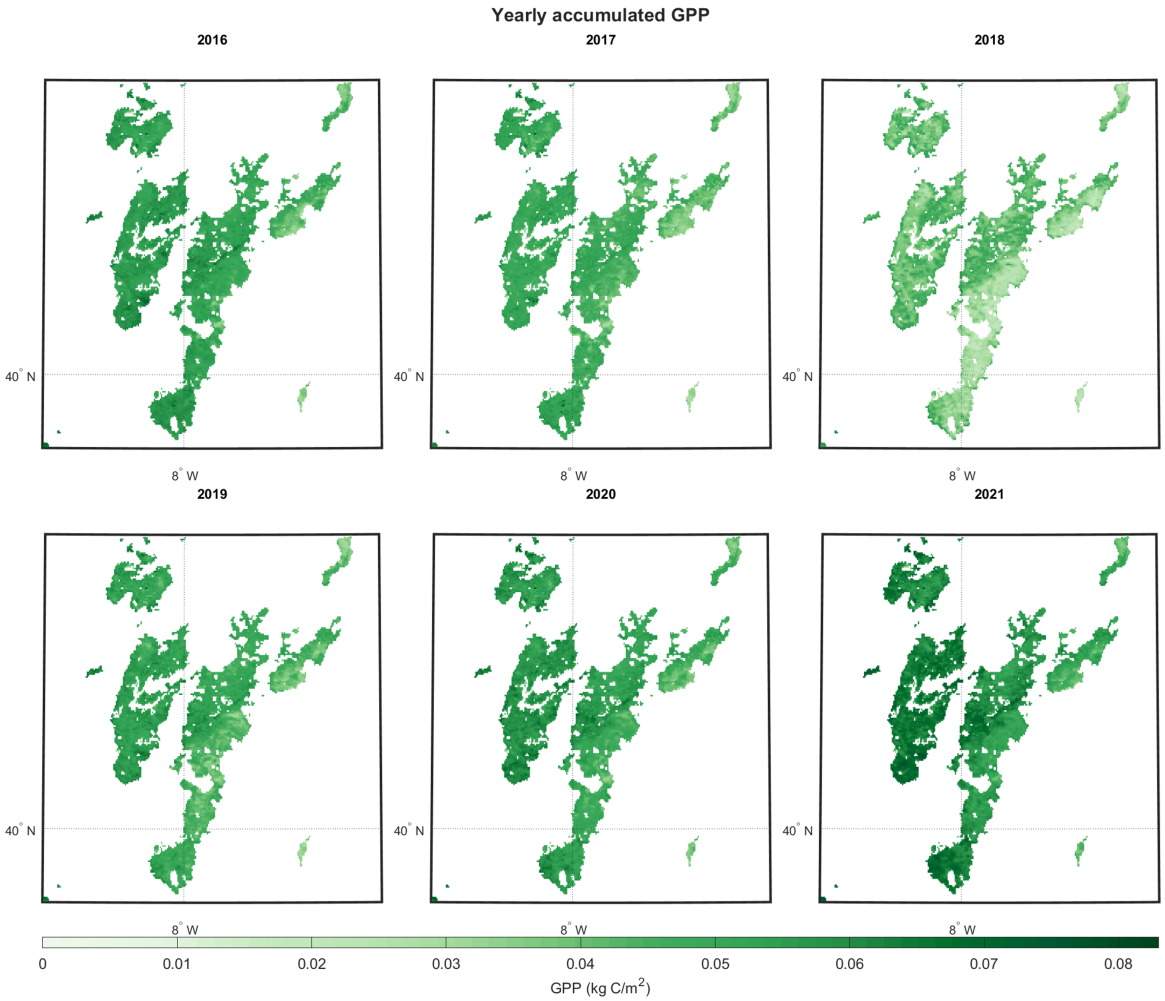

Figure 3.25: Central Region burnt area accumulated GPP evolution 2016-2021.

As for the case of Monchique, the year before the fire was chosen to evaluate the land cover types that burnt. From Figure 3.26, we can see that most of the area burnt was dominated by Savanas and ENF, being Savannas the most prominent land cover type in the area. We again analysed the vegetation recovery considering the whole burnt area, the different types of land cover, and two subareas that are depicted in Figure 3.27. The majority of the vegetation enclosed by the black line (B) is composed of ENF, as seen in Figure 3.27 (this area is adjacent to the Pedrogão Grande area which burnt in June of the same year). The vegetation in the area delimited by the red line (A) encompasses a mixture of Savannas and ENF and covers a large extent of the burnt scar.

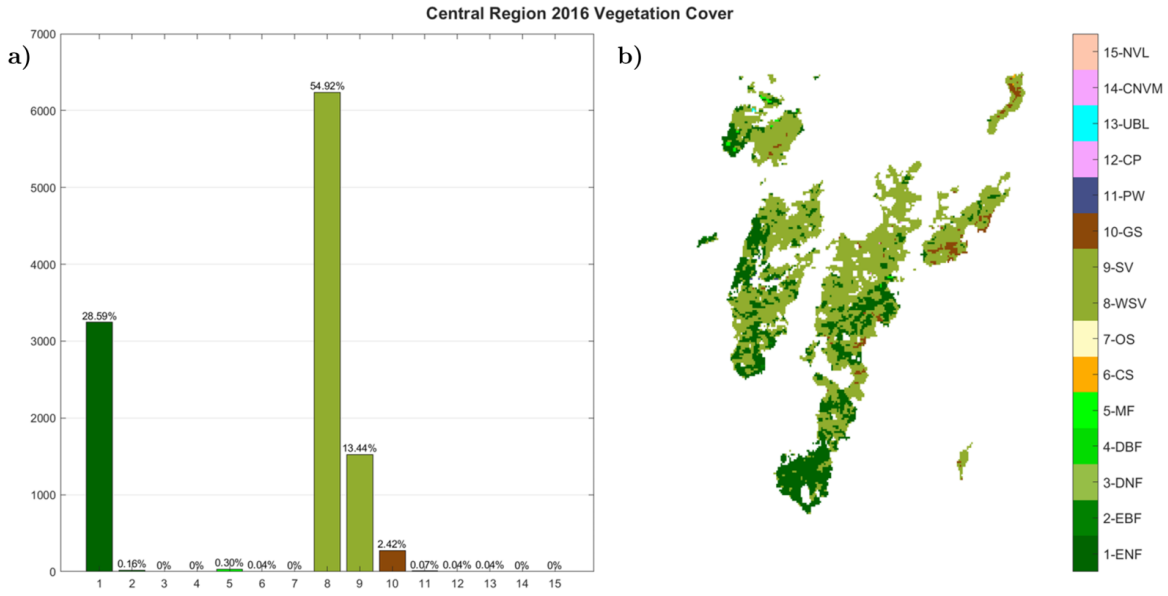

Figure 3.26: Central Region burnt area a) percentage of each land cover type and b) the land cover distribution for the year that preceded the fire (2016).

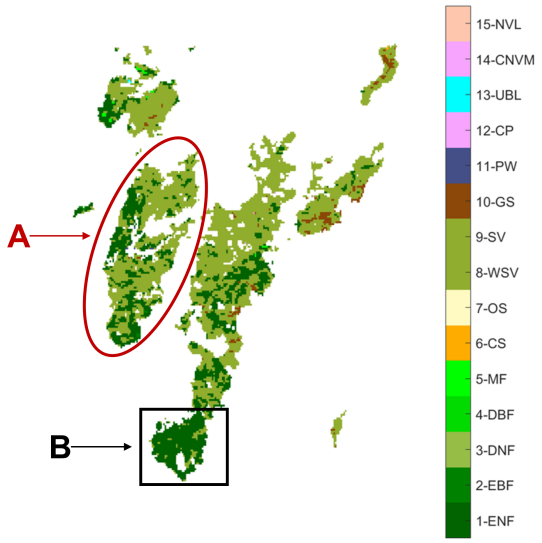

Figure 3.27: Burnt area in the Central region of Portugal in 2017. The red and black lines delimit two subareas (A and B, respectively) considered in the analysis.

First, the curve for the whole area was projected and the results are present in Figure 3.28. Before assessing the results of the linear regression is important to note the spike in the anomaly values in 2018. A value close to zero in the anomaly means that the GPP for that composite is very close to the GY value. This spike may be associated with the growth of transitional vegetation that are known to grow in the post-fire period (Retana et al., 2002; Lloret and Vilà, 2003). This growth spurt occurred in July and was enhanced by the high levels of precipitation during the 2018 spring, more specifically during March, which registered the second-highest value of precipitation in Portugal

since 1931 (IPMA, 2019). It should be noted that this value promptly drops as the August of that year was the second hotter and drier since 1931, only behind August 2003.

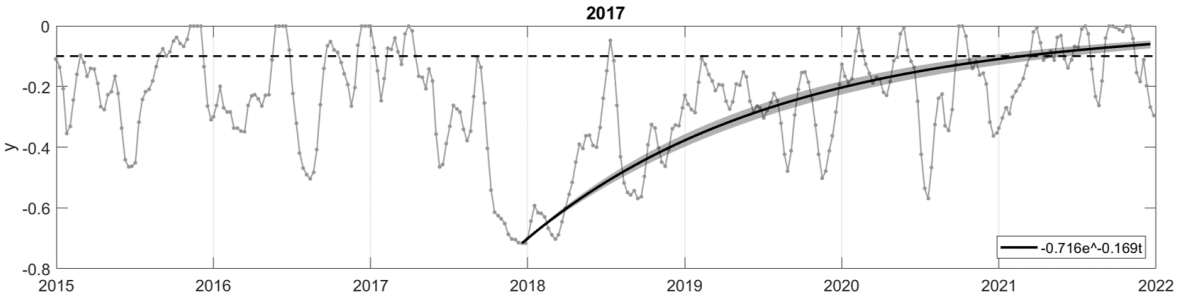

Figure 3.28: Time series of observed (lines with asterisks) and modelled (thick curves) values of 8-day composite values of lack of carbon uptake, y, over the whole 2017 Central Region burnt area. The shaded bands indicate the 95% confidence intervals. The horizontal dashed line represents the level of vegetation recovery defined as y(t)=-0.1. (The analytical expression of the fitted curves are given in the lower right corner of each panel, with the unity time, t, equal to 100 days.) $tR = 39 \pm 4\, months$

The vegetation in this area presented recovery times of thirty-nine months. This is considerably less time than the results obtained for the burnt area of Monchique in 2003. This could be explained by the wet spring of the year following the fire. In 2004 a big drought hit Portugal, therefore the water availability was scarce. On the contrary, 2018 had much more water availability due to the occurrence of many precipitation events during the vegetation growing season.

As in the previous case study, the most prominent land cover types were identified and the model was applied to them (Figure 3.29 and Table 3.7).

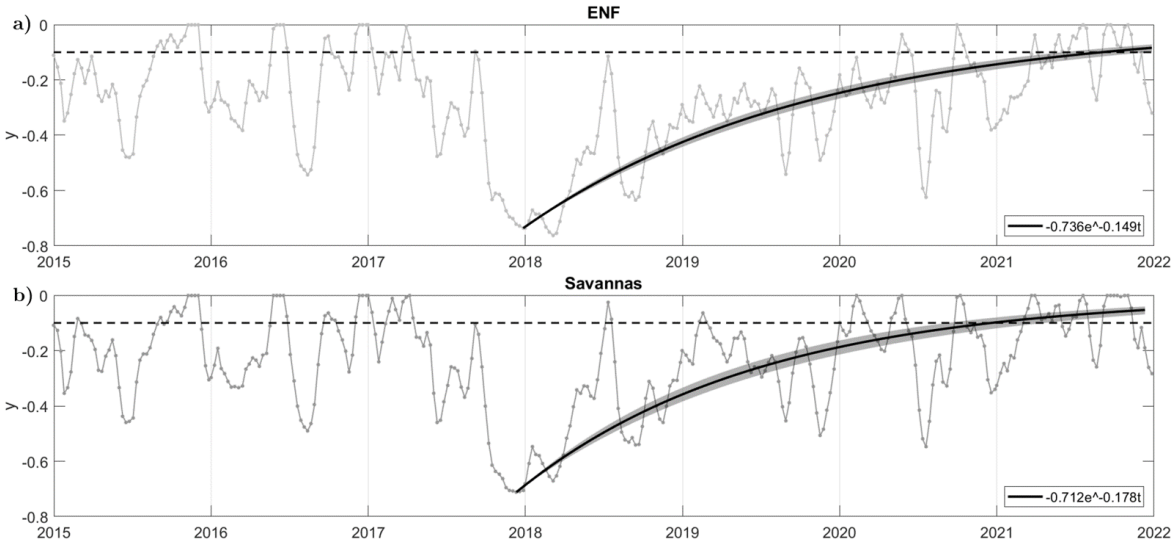

Figure 3.29: Time series of observed (lines with asterisks) and modelled (thick curves) values of 8-day composite values of lack of carbon uptake, y, over the most prominent land covers in the 2017 Central region burnt area: a) Evergreen Needleleaf Forests (ENF) and b) Savannas (SV and WSV). The shaded bands indicate the 95% confidence intervals. The horizontal dashed line represents the level of vegetation recovery defined as y(t)=-0.1. (The analytical expression of the fitted curves are given in the lower right corner of each panel, with the unity time, t, equal to 100 days.)

Table 3.7: Recovery times and and 95% confidence intervals for the most prominent land cover types in 2017 Central Region burnt area.

	tR	I95 [tR]
ENF	45	[42,48]
Savannas	37	[34,41]

The ENF have a recovery time of forty-five months, which agrees with the results obtained for the whole area, as this type of vegetation cover has recovered faster here than in 2003. Regarding the Savannas, there is an even bigger difference in the recovery time, as this region recovered twelve months faster than the 2003 counterpart. This is due to the climatological factors enunciated earlier, in addition to the fact that the majority of Savannas in this area are WSV, which have 30-60% cover of trees while in the Monchique area the majority was 10-30% cover of trees.

Area A is mainly dominated by Savannas followed by ENF. So, the recovery times should be very close to the total area. And, in fact, that is the case, as this area presents recovery times of thirty-nine months, with the 95% confidence level ranging from thirty-six to forty-two months as we can see in Figure 3.30 and Table 3.8.

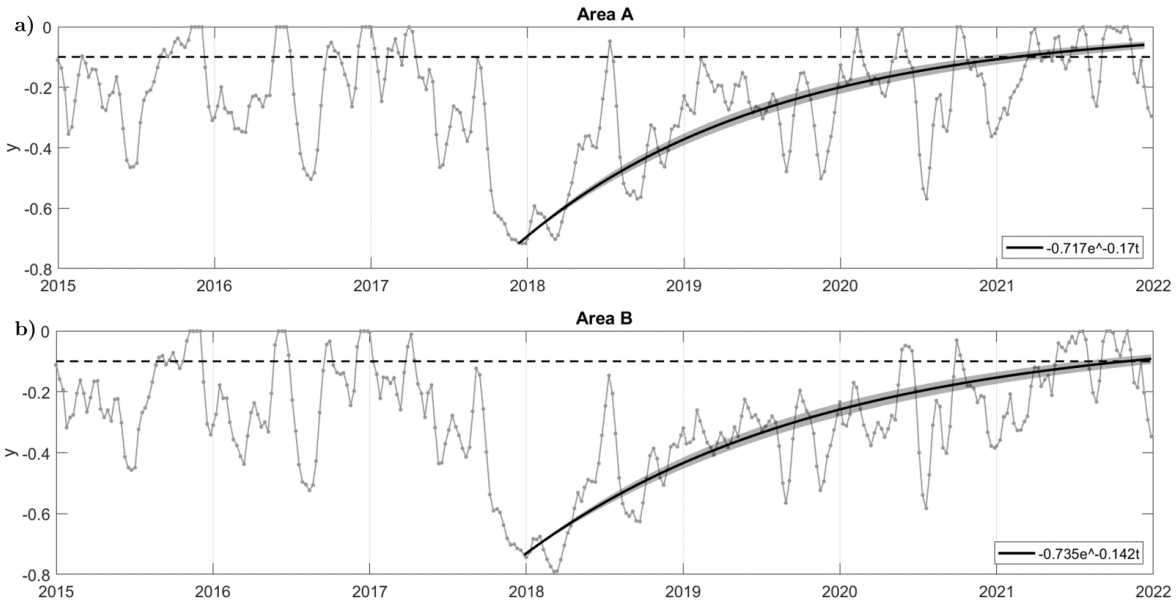

Figure 3.30: Time series of observed (lines with asterisks) and modelled (thick curves) values of 8-day composite values of lack of carbon uptake, y, over subareas a) A and b) B of the 2017 Central Region burnt area. The shaded bands indicate the 95% confidence intervals. The horizontal dashed line represents the level of vegetation recovery defined as y(t)=-0.1. (The analytical expression of the fitted curves are given in the lower right corner of each panel, with the unity time, t, equal to 100 days.)

Table 3.8: Recovery times and and 95% confidence intervals for subareas A (red delimited) and B (black delimited) of the 2017 Central Region burnt area.

	tR	I95 [tR]
Area A	39	[36,42]
Area B	47	[43,51]

For area B (Figure 3.30 and Table 3.8), ENF was the dominant land cover type, so the recovery times should be very close to the values obtained for this land cover in the whole area. In fact, the values are very close, as this area has recovered in forty-seven months, which is two months more than the results obtained for the ENF in the whole area. Important to note that for the application of the model to this are there was a need to adjust the minimum value of NPP, as the absolute minimum was during 2018 this was maybe due to the drought effects that affected the area in 2016-2017 and the early months of 2018.

4

Conclusions and Final Remarks

This study aims to analyse how wildfires and droughts impact vegetation productivity, as obtained by vegetation's gross and net primary production in the Iberian Peninsula. The vegetation response to extreme events was studied, first by performing a climatological study of the Iberian Peninsula and then by applying a vegetation recovery model (initially used by Gouveia et al. (2010) with NDVI data) to a GPP data input. The climatological analysis showed clearly how the vegetation productivity in the Iberia is impacted by recurrent drought events and wildfires. Moreover, the vegetation recovery model was successfully adapted to be used with GPP data, and it was used to characterise the recovery of vegetation productivity after two wildfires in areas of high susceptibility for the occurrence of severe fires.

From the NPP maps we identified burnt areas as in the years after the fire the affected areas presented a decrease in production values. The drastic decrease of NPP in burnt areas results in an increase of its time variance. To perform an analysis of the impacts of climate events alone, regions with very high NPP variance were flagged and not included in the series constructed to analyse the climate factors.

A cluster analysis was performed over the NPP data, excluding the flagged high variance pixels, albeit we do not find an objective criterion for a precise number of clusters to be defined, the use of a number of five proved to divide the Iberian Peninsula into geographic coherent regions, presenting distinct vegetative cycles that represents the main vegetation types present in the different clusters. The North and Northwest of the Iberian Peninsula proved to be the most productive clusters, which agrees with the land cover distribution since these two are mainly covered by Savannas and Evergreen Needleleaf Forests, which are highly productive vegetation types. The clusters which extend from the Northeastern to the Eastern Iberian Peninsula, including a Central region, showed a positive trend in the NPP over the last twenty years. It is suggested

that the positive trend may be related to changes in the type of vegetation with part of the Grasslands area being replaced by Savannas and Evergreen Needleleaf Forests which are more productive vegetation types.

However, to state this without doubt, a different Land Cover classification with higher spatial resolution and better adapted to the reality of the Iberian Peninsula climate and vegetation distribution would need to be employed, such as the recent COSc maps (available at DGT (2021)).

In Portugal's vegetation cover a noticeable decrease in Evergreen Needleleaf Forests was detected in 2017, this could be related to the vegetation type change imposed by the 2017 wildfires. However, this is likely not the only reason for this, as we found that more underlying issues may have occurred here. But, in order to identify these issues, again a different Land Cover classification more suitable for studying vegetation cover changes needs to be used.

The Portuguese burnt areas for the four years of large number of wildfires (2003, 2005, 2012 and 2017) showed strong NPP negative anomalies in the year of occurrence of wildfires and in the subsequent year. Because the wildfires tend to occur more associated with droughts and high temperatures, in some cases their impacts on the annual NPP are not seen clearly separated from the impacts of the climatic factors. The analysis of GPP 8-day data provides much more clear evidence of wildfires impacts.

We started the application of the vegetation recovery model on GPP data with an analysis of the sensitivity to the number of years included in the fitting period. The results indicate that a period of four years is a good compromise between a long enough window to assess the vegetation recovery, but short enough to not induce more external effects in the recovery time estimates.

The application of the recovery model, to the burnt areas of the wildfires in Monchique in 2003 gives consistent estimate of 47 months for each of the three different sub-areas. Applying the recovery model to different vegetation types showed a distinct recovery time for Grassland. In fact, Evergreen Needleleaf Forests, Evergreen Broadleaf Forests and Savannas showed similar results (51, 50 and 49 months respectively) while the less productive Grasslands had a faster recovery time of 41 months. The obtained recovery times for the burnt areas of Monchique in 2003 were compared with the results obtained by Gouveia et al. (2010) for the same area but using NDVI data and a different time window. The recovery times calculated here are very similar to the results obtained by Gouveia et al. (2010). This shows the robustness of the model.

The vegetation productivity in the global burnt areas of the wildfires of October 2017 showed significantly faster recovery times (39 months) than the vegetation productivity in the burnt area of Monchique in 2003. One reason for this discrepancy is that after the Monchique wildfires a drought occurred that spanned from 2004 to 2005 affecting

the recovery of the vegetation. Meanwhile, the 2017 wildfires coincided with the end of the 2016-2017 drought, however, the 2018 spring and early summer were very wet and therefore more favourable for vegetation growth and development. An analysis of the recovery time of vegetation productivity, partitioning the burnt area according to the vegetation type before the fire revealed that the areas previously occupied by Evergreen Needleleaf Forests had longer recovery time (45 months) than the areas previously occupied by Savannas (37 months).

Because, when the analysis is made on different regions (subareas of the burnt area), diverse vegetation types may be present in different proportions, the recovery time may also depend on the chosen subarea. We tested this by fitting the model for two subareas in the Centre region of Portugal, designated as areas A and B. The recovery time of the vegetation productivity of area A and B were 39 and 47 months, respectively. The difference agrees with the difference obtained for the two vegetation types analysed above. In fact area A is predominantly covered by Savannas whereas area B is predominantly occupied by ENF.

In conclusion, the work helped to better understand the response of vegetation to extreme events, like droughts and wildfires. It was also noted that different vegetation types respond differently to these adverse events. For this, the adaptation of the model proved to be invaluable to assess the vegetation recovery time.

Regarding future work, a land cover dataset with better resolution and more specific vegetation cover types adapted to the climatic condition of the Iberian Peninsula should be employed to better understand how the vegetation cover has changed during the considered period. This is very important because the used Land Cover dataset does not possess the required resolution to understand some of the vegetation cover changes that occurred in the past few years, like the intensive agriculture in Alentejo that has been mentioned by some authors and broadly mentioned on social media. Further analysis of the vegetative cycle for vegetation of each land cover type will help to better understand the impact of fires, droughts and land cover change on vegetation productivity.

References

Allen H., Simonson W., Parham E., Santos E.d.B.e. and Hotham P. (2018). Satellite remote sensing of land cover change in a mixed agro-silvo-pastoral landscape in the alentejo, portugal. *International Journal of Remote Sensing*, 39(14):4663–4683.

AppEEARS (2022). Application for extracting and exploring analysis ready samples (appeears). ver. 2.74. nasa eosdis land processes distributed active archive center (lp daac), usgs/earth resources observation and science (eros) center, sioux falls, south dakota, usa. url: `https://lpdaacsvc.cr.usgs.gov/appeears`. Acessed: 2022-09-23.

Ayarzagüena B., Barriopedro D., Garrido-Perez J., Abalos M., de la Cámara A., García-Herrera R., Calvo N. and Ordóñez C. (2018). Stratospheric connection to the abrupt end of the 2016/2017 iberian drought. *Geophysical Research Letters*, 45(22):12–639.

Bastos A., Gouveia C., DaCamara C. and Trigo R. (2011). Modelling post-fire vegetation recovery in portugal. *Biogeosciences*, 8(12):3593–3607.

Bonan G.B., Levis S., Kergoat L. and Oleson K.W. (2002). Landscapes as patches of plant functional types: An integrating concept for climate and ecosystem models. *Global Biogeochemical Cycles*, 16(2):5–1.

Bond W.J., Woodward F.I. and Midgley G.F. (2005). The global distribution of ecosystems in a world without fire. *New phytologist*, 165(2):525–538.

Campioli M., Malhi Y., Vicca S., Luyssaert S., Papale D., Peñuelas J., Reichstein M., Migliavacca M., Arain M. and Janssens I.A. (2016). Evaluating the convergence between eddy-covariance and biometric methods for assessing carbon budgets of forests. *Nature communications*, 7(1):1–12.

Chuvieco E., Lizundia-Loiola J., Pettinari M.L., Ramo R., Padilla M., Tansey K., Mouillot F., Laurent P., Storm T., Heil A. et al. (2018). Generation and analysis of a new global burned area product based on modis 250 m reflectance bands and thermal anomalies. *Earth System Science Data*, 10(4):2015–2031.

Chuvieco E., Yue C., Heil A., Mouillot F., Alonso-Canas I., Padilla M., Pereira J.M., Oom D. and Tansey K. (2016). A new global burned area product for climate assessment of fire impacts. *Global Ecology and Biogeography*, 25(5):619–629.

Cowling R.M., Rundel P.W., Lamont B.B., Arroyo M.K. and Arianoutsou M. (1996). Plant diversity in mediterranean-climate regions. *Trends in Ecology & Evolution*, 11(9):362–366.

DGT (2021). Carta de ocupação do solo conjuntural - 2021. url: `https://snig.dgterritorio.gov.pt/rndg/srv/search?keyword=COSc`. Acessed: 2022-09-23.

Díaz-Delgado R., Lloret F., Pons X. and Terradas J. (2002). Satellite evidence of decreasing resilience in mediterranean plant communities after recurrent wildfires. *Ecology*, 83(8):2293–2303.

Díaz-Delgado R. and Pons X. (2001). Spatial patterns of forest fires in catalonia (ne of spain) along the period 1975–1995: Analysis of vegetation recovery after fire. *Forest ecology and management*, 147(1):67–74.

Díaz-Delgado R., Salvador R. and Pons X. (1998). Monitoring of plant community regeneration after fire by remote sensing. *Fire management and landscape ecology*, 315–324.

ESA (2018). Spot - vegetation programme. url: `https://www.spot-vegetation.com/`. Acessed: 2022-09-23.

ESA (2022a). Explore vegetation (vgt). url: `https://earth.esa.int/eogateway/instruments/vegetation-proba-v`. Acessed: 2022-09-23.

ESA (2022b). Proba-1 overview. url: `https://www.esa.int/Applications/Observing_the_Earth/Proba-1_overview`. Acessed: 2022-09-23.

ESA (2022c). Spot. url: `https://earth.esa.int/eogateway/missions/spot`. Acessed: 2022-09-23.

Exbrayat J.F., Bloom A.A., Carvalhais N., Fischer R., Huth A., MacBean N. and Williams M. (2019). Understanding the land carbon cycle with space data: current status and prospects. *Surveys in Geophysics*, 40(4):735–755.

Field C.B., Randerson J.T. and Malmström C.M. (1995). Global net primary production: combining ecology and remote sensing. *Remote sensing of Environment*, 51(1):74–88.

Frank D., Reichstein M., Bahn M., Thonicke K., Frank D., Mahecha M.D., Smith P., Van der Velde M., Vicca S., Babst F. et al. (2015). Effects of climate extremes on the terrestrial carbon cycle: concepts, processes and potential future impacts. *Global change biology*, 21(8):2861–2880.

Friedlingstein P., Jones M.W., O'Sullivan M., Andrew R.M., Bakker D.C., Hauck J., Le Quéré C., Peters G.P., Peters W., Pongratz J. et al. (2022). Global carbon budget 2021. *Earth System Science Data*, 14(4):1917–2005.

García-Herrera R., Hernández E., Barriopedro D., Paredes D., Trigo R.M., Trigo I.F. and Mendes M.A. (2007). The outstanding 2004/05 drought in the iberian peninsula: associated atmospheric circulation. *Journal of Hydrometeorology*, 8(3):483–498.

Gilgen A.K. and Buchmann N. (2009). Response of temperate grasslands at different altitudes to simulated summer drought differed but scaled with annual precipitation. *Biogeosciences*, 6(11):2525–2539.

Giovos R., Tassopoulos D., Kalivas D., Lougkos N. and Priovolou A. (2021). Remote sensing vegetation indices in viticulture: a critical review. *Agriculture*, 11(5):457.

Gouveia C., Bastos A., Trigo R. and DaCamara C. (2012). Drought impacts on vegetation in the pre-and post-fire events over iberian peninsula. *Natural Hazards and Earth System Sciences*, 12(10):3123–3137.

Gouveia C., DaCamara C. and Trigo R. (2010). Post-fire vegetation recovery in portugal based on spot/vegetation data. *Natural Hazards and Earth System Sciences*, 10(4):673–684.

Gouveia C., Páscoa P. and DaCamara C. (2018). Post-fire vegetation recovery in iberia based on remote-sensing information. *Forest Fire*, 113–130.

Gouveia C., Trigo R. and DaCamara C. (2009). Drought and vegetation stress monitoring in portugal using satellite data. *Natural Hazards and Earth System Sciences*, 9(1):185–195.

Hagolle O., Lobo A., Maisongrande P., Cabot F., Duchemin B. and De Pereyra A. (2005). Quality assessment and improvement of temporally composited products of remotely sensed imagery by combination of vegetation 1 and 2 images. *Remote Sensing of Environment*, 94(2):172–186.

Hansen M.C., DeFries R.S., Townshend J.R. and Sohlberg R. (2000). Global land cover classification at 1 km spatial resolution using a classification tree approach. *International journal of remote sensing*, 21(6-7):1331–1364.

ICNF (2017). Relatório provisório de incêndios florestais - 2017. url: `https://www.icnf.pt/api/file/doc/7b89239f0e8506f2`. Acessed: 2022-09-23.

ICNF (2018). Relatório de estabilização de emergência do incêndio de monchique de agosto de 2018. url: `https://www.icnf.pt/api/file/doc/b324f8e41c231899`. Acessed: 2022-09-23.

IPMA (2019). Boletim climatológico anual portugal continental 2018. url: `https://www.ipma.pt/resources.www/docs/im.publicacoes/edicoes.online/20190131/ddliTNijyEWyfrhUMDTy/cli_20180901_20181231_pcl_aa_co_pt.pdf`. Acessed: 2022-09-23.

Jacquemoud S. and Baret F. (1990). Prospect: A model of leaf optical properties spectra. *Remote sensing of environment*, 34(2):75–91.

Keeley S.C., Keeley J.E., Hutchinson S.M. and Johnson A.W. (1981). Postfire succession of the herbaceous flora in southern california chaparral. *Ecology*, 62(6):1608–1621.

Kemanian A.R., Stöckle C.O. and Huggins D.R. (2004). Variability of barley radiation-use efficiency. *Crop science*, 44(5):1662–1672.

Liberato M.L., Montero I., Gouveia C., Russo A., Ramos A.M. and Trigo R.M. (2021). Rankings of extreme and widespread dry and wet events in the iberian peninsula between 1901 and 2016. *Earth System Dynamics*, 12(1):197–210.

Lizundia-Loiola J., Otón G., Ramo R. and Chuvieco E. (2020). A spatio-temporal active-fire clustering approach for global burned area mapping at 250 m from modis data. *Remote Sensing of Environment*, 236:111493.

Lloret F. and Vilà M. (2003). Diversity patterns of plant functional types in relation to fire regime and previous land use in mediterranean woodlands. *Journal of Vegetation Science*, 14(3):387–398.

Loveland T.R. and Belward A. (1997). The international geosphere biosphere programme data and information system global land cover data set (discover). *Acta Astronautica*, 41(4-10):681–689.

Lucht W., Prentice I.C., Myneni R.B., Sitch S., Friedlingstein P., Cramer W., Bousquet P., Buermann W. and Smith B. (2002). Climatic control of the high-latitude vegetation greening trend and pinatubo effect. *Science*, 296(5573):1687–1689.

Marchetti M., Ricotta C. and Volpe F. (1995). A qualitative approach to the mapping of post-fire regrowth in mediterranean vegetation with landsat tm data. *International Journal of Remote Sensing*, 16(13):2487–2494.

Monteith J. (1972). Solar radiation and productivity in tropical ecosystems. *Journal of applied ecology*, 9(3):747–766.

Myneni R. (2020). Modis collection 6 (c6) lai/fpar product user's guide. url: `https://lpdaac.usgs.gov/documents/624/MOD15_User_Guide_V6.pdf`. Acessed: 2022-09-23.

Myneni R.B., Hall F.G., Sellers P.J. and Marshak A.L. (1995). The interpretation of spectral vegetation indexes. *IEEE Transactions on Geoscience and remote Sensing*, 33(2):481–486.

Myneni R.B., Hoffman S., Knyazikhin Y., Privette J., Glassy J., Tian Y., Wang Y., Song X., Zhang Y., Smith G. et al. (2002). Global products of vegetation leaf area and fraction absorbed par from year one of modis data. *Remote sensing of environment*, 83(1-2):214–231.

NASA (2022). Modis web. url: `https://modis.gsfc.nasa.gov/about/`. Acessed: 2022-09-23.

Nemani R.R., Keeling C.D., Hashimoto H., Jolly W.M., Piper S.C., Tucker C.J., Myneni R.B. and Running S.W. (2003). Climate-driven increases in global terrestrial net primary production from 1982 to 1999. *science*, 300(5625):1560–1563.

RAYMOND HUNT E. JR (1994). Relationship between woody biomass and par conversion efficiency for estimating net primary production from ndvi. *International Journal of Remote Sensing*, 15(8):1725–1729.

Reichstein M., Bahn M., Ciais P., Frank D., Mahecha M.D., Seneviratne S.I., Zscheischler J., Beer C., Buchmann N., Frank D.C. et al. (2013). Climate extremes and the carbon cycle. *Nature*, 500(7462):287–295.

Retana J., Maria Espelta J., Habrouk A., Luis OrdoÑEz J. and de Solà-Morales F. (2002). Regeneration patterns of three mediterranean pines and forest changes after a large wildfire in northeastern spain. *Ecoscience*, 9(1):89–97.

Röder A., Hill J., Duguy B., Alloza J.A. and Vallejo R. (2008). Using long time series of landsat data to monitor fire events and post-fire dynamics and identify driving factors. a case study in the ayora region (eastern spain). *Remote sensing of environment*, 112(1):259–273.

Roerink G.J., Menenti M., Soepboer W. and Su Z. (2003). Assessment of climate impact on vegetation dynamics by using remote sensing. *Physics and Chemistry of the Earth, Parts A/B/C*, 28(1-3):103–109.

Rouse Jr J., Haas R.H., Deering D., Schell J. and Harlan J.C. (1974). Monitoring the vernal advancement and retrogradation (green wave effect) of natural vegetation. Tech. Rep.

Running S. and Zhao M. (2019). User's guide daily gpp and annual npp (mod17a2h/a3h) and year-end gapfilled (mod17a2hgf/a3hgf) products nasa earth observing system modis land algorithm (for collection 6). url: `https://lpdaac.usgs.gov/documents/495/MOD17_User_Guide_V6.pdf`. Acessed: 2022-09-23.

Running S.W., Nemani R.R., Heinsch F.A., Zhao M., Reeves M. and Hashimoto H. (2004). A continuous satellite-derived measure of global terrestrial primary production. *Bioscience*, 54(6):547–560.

Running S.W., Thornton P.E., Nemani R. and Glassy J.M. (2000). Global terrestrial gross and net primary productivity from the earth observing system. In *Methods in ecosystem science*. Springer, 44–57.

Ryan M.G. (1991). Effects of climate change on plant respiration. *Ecological Applications*, 1(2):157–167.

Sharma S. (1995). Applied multivariate techniques. Wiley.

Silveira A., Ferrão J., Munoz-Rojas Morenes J., Pinto-Correia T., Guimarães M.H. and Schmidt L. (2018). The sustainability of agricultural intensification in the early 21st century: insights from the olive oil production in alentejo (southern portugal). *Changing societies: legacies and challenges. Vol. 3. The diverse worlds of sustainability*, 247–275.

Sulla-Menashe D. and Friedl M. (2018). User guide to collection 6 modis land cover (mcd12q1 and mcd12c1) product. url: `https://lpdaac.usgs.gov/documents/101/MCD12_User_Guide_V6.pdf`. Acessed: 2022-09-23.

Tang J., Luyssaert S., Richardson A.D., Kutsch W. and Janssens I.A. (2014). Steeper declines in forest photosynthesis than respiration explain age-driven decreases in forest growth. *Proceedings of the National Academy of Sciences*, 111(24):8856–8860.

Turner D.P., Ritts W.D., Cohen W.B., Gower S.T., Zhao M., Running S.W., Wofsy S.C., Urbanski S., Dunn A.L. and Munger J. (2003). Scaling gross primary production (gpp) over boreal and deciduous forest landscapes in support of modis gpp product validation. *Remote Sensing of Environment*, 88(3):256–270.

Úbeda X., Outeiro L. and Sala M. (2006). Vegetation regrowth after a differential intensity forest fire in a mediterranean environment, northeast spain. *Land Degradation & Development*, 17(4):429–440.

van der Molen M.K., Dolman A.J., Ciais P., Eglin T., Gobron N., Law B.E., Meir P., Peters W., Phillips O.L., Reichstein M. et al. (2011). Drought and ecosystem carbon cycling. *Agricultural and Forest Meteorology*, 151(7):765–773.

Viedma O., Meliá J., Segarra D. and Garcia-Haro J. (1997). Modeling rates of ecosystem recovery after fires by using landsat tm data. *Remote Sensing of Environment*, 61(3):383–398.

Voulgarakis A. and Field R.D. (2015). Fire influences on atmospheric composition, air quality and climate. *Current Pollution Reports*, 1(2):70–81.

Ward D., Kloster S., Mahowald N., Rogers B., Randerson J. and Hess P. (2012). The changing radiative forcing of fires: global model estimates for past, present and future. *Atmospheric Chemistry and Physics*, 12(22):10857–10886.

Wu D., Zhao X., Liang S., Zhou T., Huang K., Tang B. and Zhao W. (2015). Time-lag effects of global vegetation responses to climate change. *Global change biology*, 21(9):3520–3531.

Xue J. and Su B. (2017). Significant remote sensing vegetation indices: A review of developments and applications. *Journal of sensors*, 2017.

Zavalloni C., Gielen B., Lemmens C., De Boeck H., Blasi S., Van den Bergh S., Nijs I. and Ceulemans R. (2008). Does a warmer climate with frequent mild water shortages protect grassland communities against a prolonged drought? *Plant and Soil*, 308(1):119–130.

Zhao M., Heinsch F.A., Nemani R.R. and Running S.W. (2005). Improvements of the modis terrestrial gross and net primary production global data set. *Remote sensing of Environment*, 95(2):164–176.

Zhao M., Running S.W. and Nemani R.R. (2006). Sensitivity of moderate resolution imaging spectroradiometer (modis) terrestrial primary production to the accuracy

of meteorological reanalyses. *Journal of Geophysical Research: Biogeosciences*, 111(G1).

Zhou L., Tucker C.J., Kaufmann R.K., Slayback D., Shabanov N.V. and Myneni R.B. (2001). Variations in northern vegetation activity inferred from satellite data of vegetation index during 1981 to 1999. *Journal of Geophysical Research: Atmospheres*, 106(D17):20069–20083.